A SILICON BASED REGENERATION ELECTRODE
FOR IMPLANTATION IN AMPHIBIA

by

CHRISTOPHER ROSE

S.B. Massachusetts Institute of Technology
(1979)

SUBMITTED IN PARTIAL FULFILLMENT OF
OF THE REQUIREMENTS FOR THE
DEGREE OF

MASTER OF SCIENCE

at the

MASSACHUSETTS INSTITUTE OF TECHNOLOGY

June 1981

Signature of Author____________________
Department of Electrical
Engineering and Computer Science
May 22, 1981

Certified by____________________ 5/22/81
Prof. Dimitri A. Antoniadis
Thesis Supervisor

Certified by____________________ 5/22/81
Dr. Steven A. Raymond
Thesis Supervisor

Accepted by____________________
Prof. Arthur C. Smith
Chairman, Department Committee

A SILICON BASED REGENERATION ELECTRODE FOR IMPLANTATION IN AMPHIBIA

by

CHRISTOPHER ROSE

Submitted to the Department of Electrical Engineering and Computer Science on May 22, 1981 in partial fulfillment of the requirements for the Degree of Master of Science in Electrical Engineering

ABSTRACT

Described herein is a procedure for constructing a silicon based 12-channel recording/stimulating electrode for use in chronic connection to peripheral nerves in amphibia or nervous tissue cultures in vitro. In peripheral nerve applications, the device falls under the general heading of "Regeneration Electrode". In such an application the electrode theoretically offers multichannel recording of neural activity in small bundles of axons within a peripheral nerve. As used in vitro, this device offers spatial sampling of electrical activity within a culture of nervous tissue.

This 12-channel electrode is fabricated using standard planar integrated circuit technology and standard microstructure technology. This fact, coupled with relatively modest (as compared to "state of the art" processing) size and tolerance requirements should ultimately allow the construction of densely packed addressable microelectrode structures using current silicon microstructure fabrication techniques.

As of this writing, the aforementioned electrode has not been tested either chronically in vivo, or in tissue culture, however, electrical tests have been conducted in a physiological saline bath.

Thesis Supervisors:	D. A. Antoniadis, Associate Prof.E.E.
	S. A. Raymond, Lecturer E.E.

ACKNOWLEDGEMENTS

I would like to thank my advisors, Professor Dimitri Antoniadis and Dr. Steven Raymond for their support and encouragement; Professors Rafael Reif and William Seibert for many helpful discussions; Mrs. Dorothy Chapman and Mr.Joseph Walsh whose assistance in the laboratory was invaluable; Andy Hawryluk, of the Microstructures Laboratory, for leading, by the hand, through reactive ion etching; and Carter Kittrell of the Massachusetts Institute of Technology Spectroscopy Laboratory for the use of their high power N-YAG laser.

In particular, I would like to thank my parents, George N. Rose and Jeanne J. Rose for their help in typing, editing, drawing figures and simply enduring the rigors of assembling this thesis.

TABLE OF CONTENTS

FIGURES

INTRODUCTION

Our goal is to interface the electrical signals transmitted on vertebrate peripheral nerves* with external recording and stimulating equipment. If access could be gained to the information carried by these nerves, chronic sampling of many fibers would extend our capacity to study how motor signals control muscle contraction and how sensory organs transmit environmental information to the central nervous system (CNS).

Since even after axotomy and ligation of a severed nerve bundle, as would be the case for an amputee, neural information is still transmitted on the nerve stump (Davis, et al 1978, Gordon et al 1979, DeLuca & Gilmore 1978), possible applications of considerable importance exist in the field of prosthetics: an artifical limb with sensory function as well as motor function, a functional artificial eye or ear. Many technological and scientific gaps make them unfeasible at present, but a two-way interface to peripheral nerves is a beginning.

A brief morphological and functional description of peripheral nerves necessary to understand the source for electrical recording and the load for stimulation follows.

Peripheral nerve bundles in vertebrates are composed of many individual fibers called axons. A cross section of a

---

*Including auditory and optical nerves.

peripheral nerve is shown in figure I-1. Such nerve bundles reach diameters of several millimeters in some mammals. Axon diameters vary from fractions of a micrometer to fifteen micrometers (Boyd & Davey 1968).

A voltage spike of approximately 100mV in amplitude called an action potential propagates along an active axon. The characteristic waveshape is shown in figure 2-3. Action potentials elicit contraction in muscle tissue and other action potentials in neural tissues via synaptic coupling. Axons are either efferent (carry signals from the CNS) or afferent (carry signals to the CNS) and may be either myelinated or unmyelinated. Myelin sheathing increases the speed of propagation of an action potential along the axon.

Ideally we would like our device to monitor activity in each individual axon as well as be capable of inducing an action potential in each axon separately. The device should not be toxic to the nerve, or worse yet, toxic to the animal. More concisely, the nerve and animal should be able to function normally in the presence of our ideal interface.

Attaining such an ideal presents many problems. Nerve bundles are packed very densely with up to 400 fibers per bundle in a frog peripheral nerve with diameter under 1mm. Ideally we would like to monitor each axon. Gaining access to an individual axon for probing without disturbing the nerve or animal is very difficult if not impossible with current techniques. Therefore, we must compromise by applying exist-

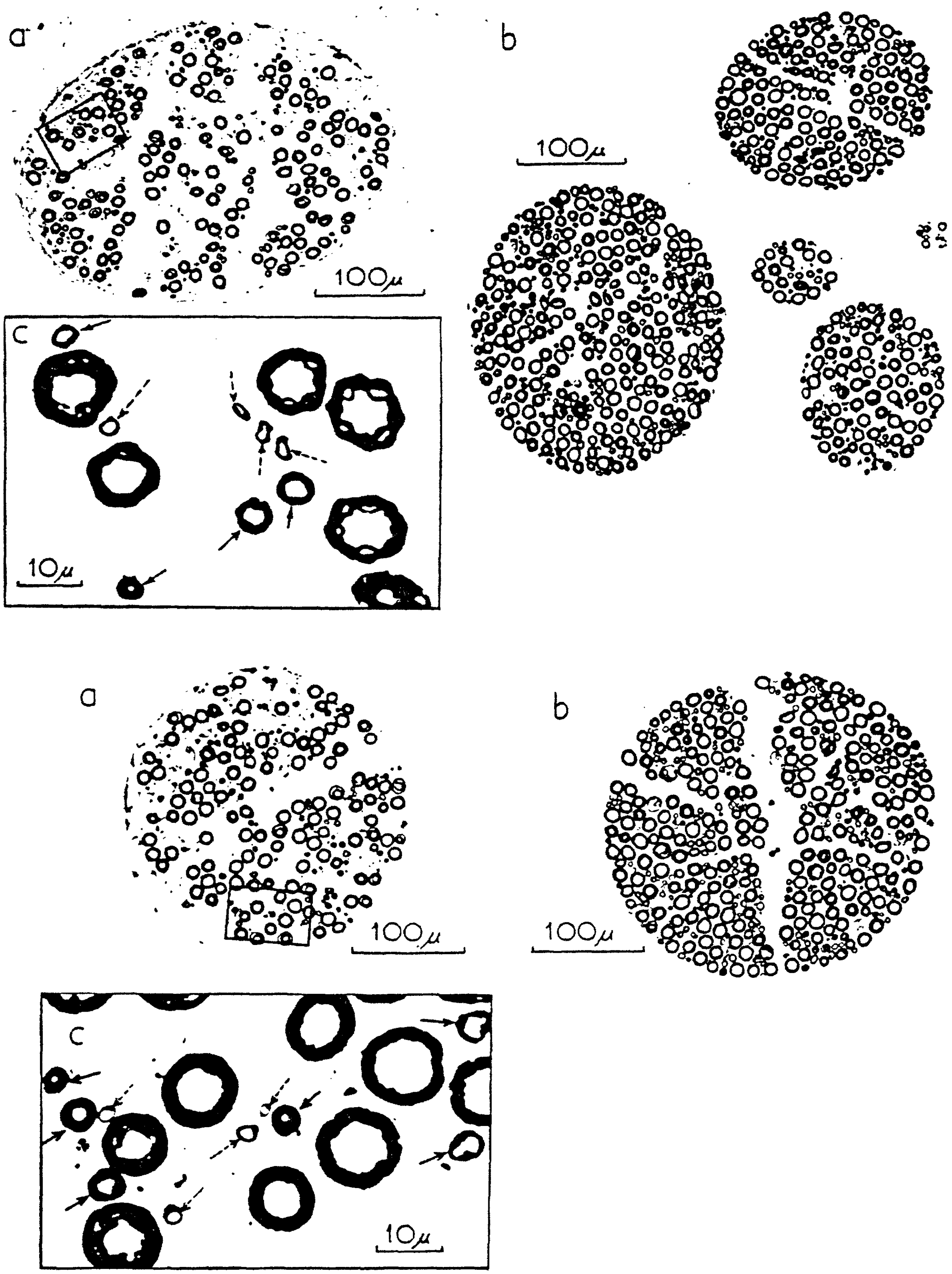

Figure I-1: Cross-section of a peripheral nerve bundle (reproduced from Boyd and Davey 1968) ing technology to the problem in novel ways. With this in mind, let us now proceed to chapter 1 where we shall examine existing neural recording/stimulation techniques with particular emphasis on their relevance to our application.

CHAPTER 1

Classically glass micropipettes filed with a suitable electrolyte have been used to make intracellular recordings. The tip diameter of these electrodes is very small, typically under .5um (Schanne & Ceretti 1978). Though they are excellent for making intracellular recordings they require almost total absence of motion and are too unwieldy for our application.

Even older than the micropipette is the noble metal wire electrode. Here, a thin wire made of a noble metal such as gold or platinum is coated with insulation except for a small length near the tip. The wire is inserted in the tissue being studied and measurements may be made. Again, however, we have a fragility problem. Coupled with this is the problem of drift in chronically implanted electrodes of this type. By "drift" is meant actual movement of the tissues relative the electrode. In our application we would not know from one day to the next which unit we were probing. This feature is particularly undesirable in a prosthetic device interface since we have presumed that particular axons control particular functions.

Another method involves a great deal of signal processing. Here,electrodes are placed in the nerve and a processor learns to recognize action potentials from particular axons. This method is based on the assumption that the action potentials of different axons, though basically the same, have slightly different waveforms and conduction velocities. Each axon has a distinct signature. Velocity correlation (Schmidt 1971), template correlation(Calvin 1973, Prochazka 1978) and linear filtering (Roberts & Hartline 1975) seem to be the means by which individual action potentials are separated from the ensemble. Velocity correlation uses only two recording electrodes but it fails to resolve superimposed action potentials (Roberts & Hartline 1975). Template correlation suffers from the same malady. Only linear filtering resolves compound events, but a problem is encountered by Roberts & Hartline who state "the number of recording electrodes must approximate the number of units present." (Roberts & Hartline 1975). If we study a nerve bundle of 400 fibers such a processing is costly at present due to the amount of computation involved in separating the action potentials. Also, though this "signature" method seems to be one of the least invasive techniques, the inverse problem of selective stimulation is not antisymmetric and therefore requires separate technological development.

The technique which has shown the most promise so far is that of the cuff electrode as illustrated in figure 1-1 (DeLuca & Gilmore 1978). Here an insulating cuff with radially symmetric noble metal electrodes on the interior face is fitted around a nerve bundle. Using signal processing techniques on the voltage waveforms obtained, "centers of activity"

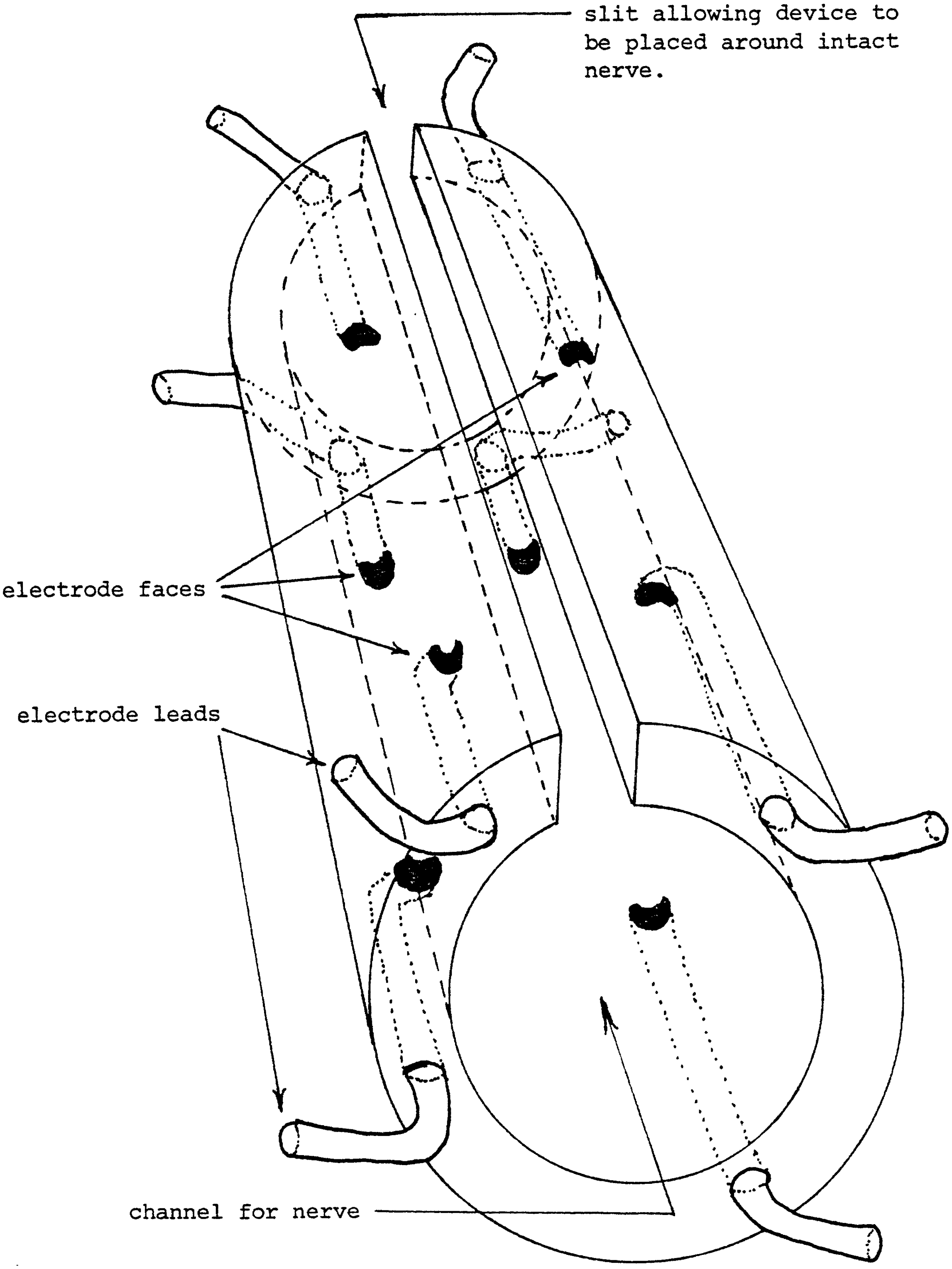

Figure 1-1: Cuff electrode

may be located within the bundle (DeLuca & Lichtenberg 1979, Stein et al 1979, Andreassen et al 1979). Since there is some morphological relation between nerve fiber placement within the bundle and the structures innervated, this type of triangulation may be used for prosthetic device control. There is virtually no drift since the device is enveloped by connective tissue after implantation (DeLuca 1978). However, the recorded signals are very small (on the order of 10uv) and thus difficult to detect above the noise level (Stein et al 1975) and again, stimulation of axons within the nerve bundle does not seem feasible to this author since there do not seem to be enough constraints imposed by the surrounding electrodes on the electric field in the cross-section. Thus it would be difficult to selectively generate fields strong enough to cause depolarization in a particular area of the nerve bundle. Nonetheless, the cuff electrode is still the most well-researched and possibly the most viable option to date.

We now come to the concept which is the basis of this thesis: the regeneration electrode. This technique capitalizes on the fact that severed nerve bundles tend to regenerate from the proximal stump (that side closest to the spinal cord) toward the muscle and sensory organs which they innervated before severance (Nesmeianova 1977, Singer & Schade 1964, Sunderland 1968, Young 1942). If a grid of small insulating channels is placed in the path of the regenerating nerve, the individual axons which comprise the nerve will grow through the channels (Mannard & Stein 1974, Stein et al 1975) in their quest for their original terminations (see figure 1-2).

Since the grid is an insulator, the axons within it are electrically isolated from one another. Also, the large volume of saline in which the axons were once bathed is restricted to that which is between the axon and the channel walls. We have laid the foundations for isolated recording/ stimulation of individual axons. We leave the actual modeling of the measurements until chapter 2.

Stein constructed his first regeneration electrode from epoxy and thin teflon coated silver wire (see figure 1-3). Stein's implantation procedure involved partially transecting a nerve bundle and placing the device in the notch thus created. After a period of two months, to allow complete regeneration, electrophysiological tests were carried out. Triphasic voltage spikes were recorded, much as would be expected for single units in such a recording situation. The expected amplitude and waveform will be compared to our case in chapter 2. Individual channel stimulation was easily accomplished (Mannard et al 1974).

This scheme offers very good channel separation and fosters selective recording and stimulation. Because of the restricted extracellular space in which the axons are placed, the recorded signal levels are much larger than those expected in a large saline bath. Also, there can be very little if

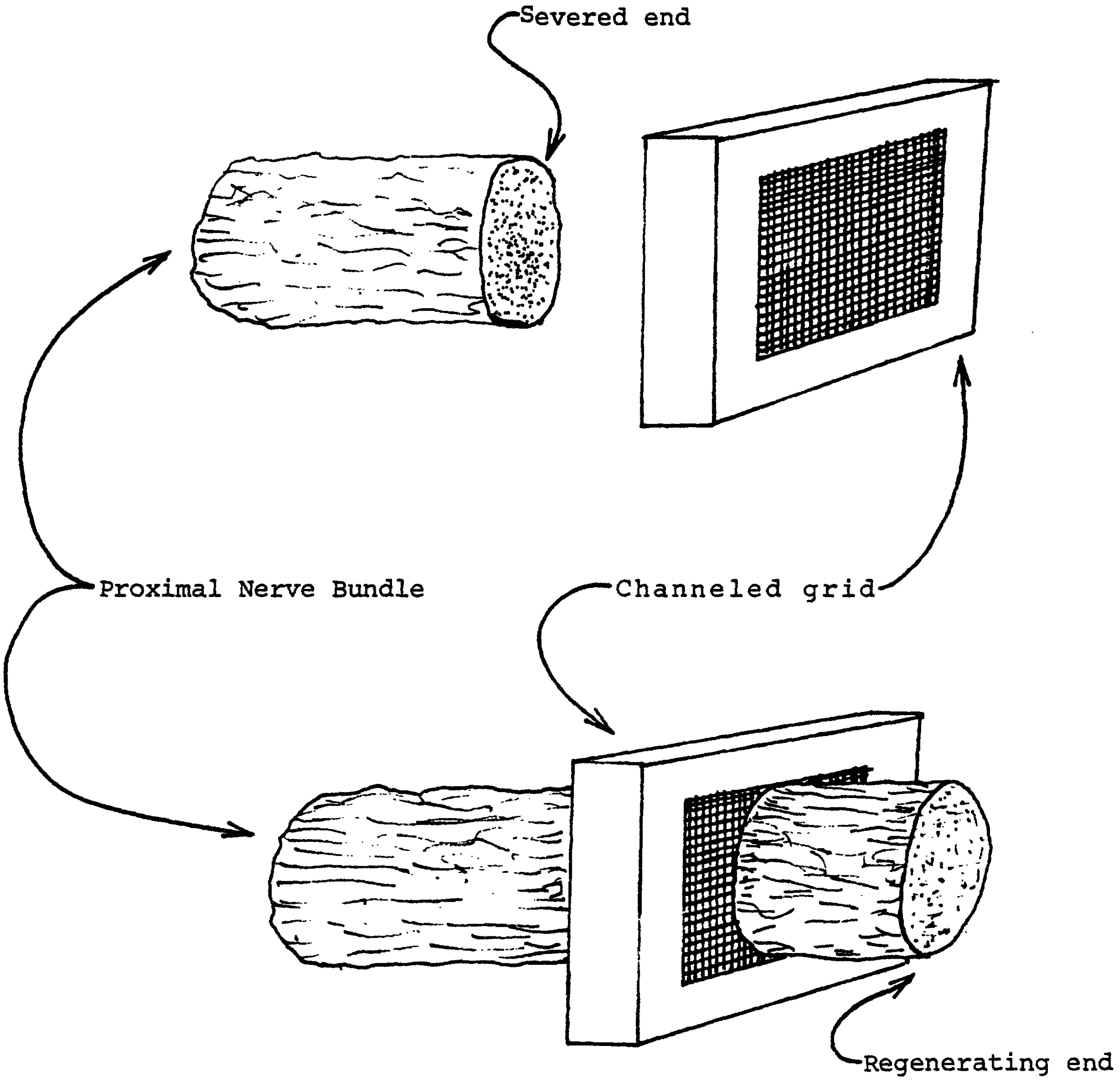

Figure 1-2: Channeled grid with regenerating nerve bundle.

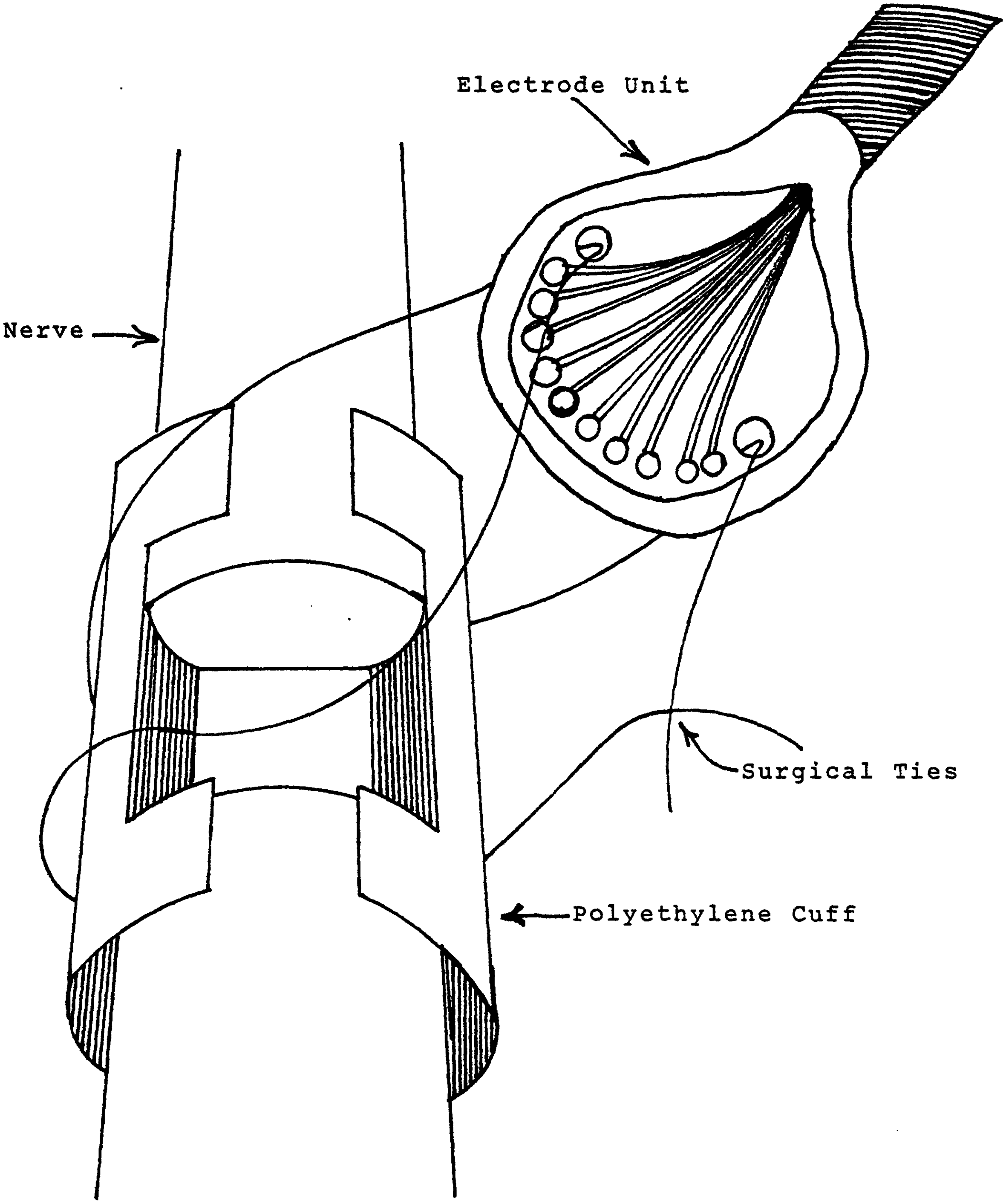

Figure 1-3: Schematic of Stein's regeneration electrode.

any drift since the axons are threaded through distinct channels.

Another type of regeneration electrode was constructed and tested by Dr. David J. Edell of U.C., Davis for his doctoral research. The thrust of his project was to apply planar integrated circuit technology to the construction of a silicon based regeneration electrode. This technique affords the placement of solid state amplifying circuitry at the recording site as well as multiplexing circuitry to decrease the number of external leads to a device with a large number of channels. A schematic of his device shown in figure 1-4. The difference between Edell's device and the regeneration electrode as previously described lies in the fact that bundles rather than individual fibers are resistively separated. A major advantage to this technique is the ease with which regenerating fibers grow through the electrode due to its short, wide channels; cross-section 160umX200um, length 140um. It seems that compound action potentials were recorded rather than single unit action potentials since distinct spikes were absent in the waveform reported. A disadvantage is seen in that Edell's metal contacts are located on the face of his device abutting a large volume of saline rather than centrally located within the channel as is the case with Stein's electrode. It is for this reason that Stein's and Edell's expected voltages differ substantially. For a large short channel of 100um diameter and 700um length as used by Stein with unmyelinated

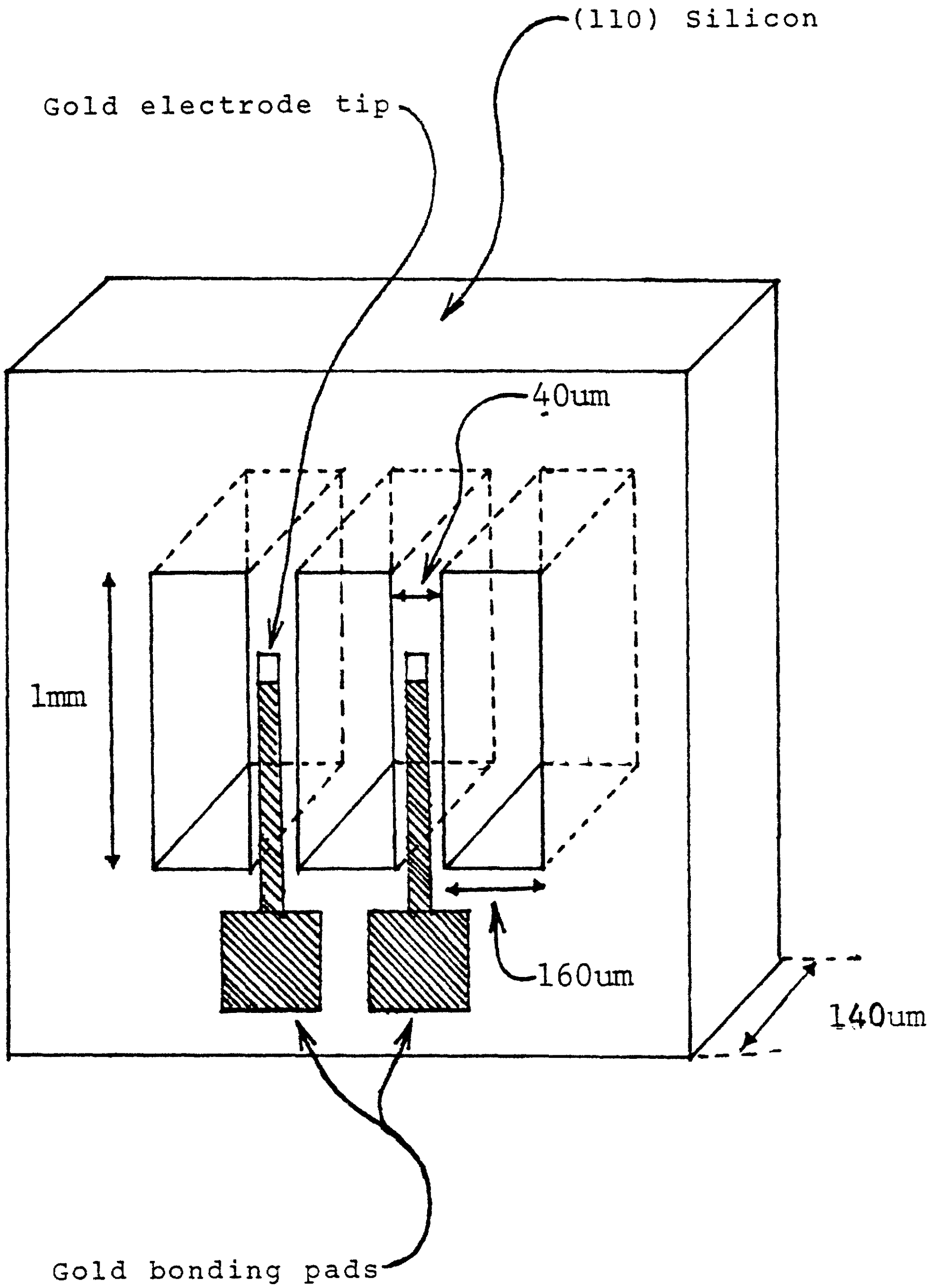

Figure 1-4: Simplified schematic of Dr. Edell's device. Not drawn to scale.

amphibian fibers, the peak voltage expected ranged from 15uV to 150uV. Actual recorded spikes were on the order of 100uV (Mannard et al 1974). As will be seen in chapter 2, this peak is proportional to the square of the length-diameter ratio so that much larger spikes could be generated using smaller, longer channels. Also, though the analysis was for unmyelinated fibers, it also extends to myelinated fibers with only a slight modification of our results (please see chapter 2).

In the case of Edell, the recorded voltage depends on the distance between the center of a node in a myelinated fiber and the electrode. For an axon 10um in diameter, if the electrode is more than 20um away from the node center, the expected peak voltage drops to 10uV and under. Since there seem to be no mechanical restraints placed on a fiber such that it must come within 20um of the recording site, spikes of 10uV would be expected. As for actual recordings, those of Edell, as mentioned previously, seemed to be compound rather than from single units hence much larger superposition voltages were recorded.

In terms of stimulation the Edell electrode is not as selective as Stein's in that all the record/stimulate sites are in contact with a common saline bath thus channel crosstalk could be increased to unacceptable levels. Edell apparently made no attempt to stimulate the nerve bundle with his electrode.

Both schemes share the unavoidable disadvantage of regeneration electrodes in that they are highly invasive, and very traumatic to both the neural tissue and the surrounding areas. Such trauma is almost certain to cause some fibrosis in the proximal end of the sectioned nerve bundle, especially in mammals. The proliferation of fibrotic tissue, if left unchecked, could occlude the channels and thereby prevent nerve regeneration through them. Nevertheless, fibrosis can be minimized by the proper choice of materials and surgical techniques, (Windle & Chambers 1951, Scott & Clemente 1955, Campbell et al 1957, Singer & Schade 1964, Nesmeianova 1977, Sunderland 1968), and fibers grow through channels 25um in diameter even in mammalian preparations (Stein et al 1975).

A problem to which there is no solution as yet is the speed of regeneration. Under the best of conditions, nerve regeneration proceeds at less than 1mm/day (Singer & Schade 1974). Couple this with a refractory period of a week or more due to the initial surgical trauma and we have the makings of a time consuming process. However, the unavailability of any measurement technique other than the cuff electrode which offers the advantages of the regeneration electrode outweighs trauma and time consideration.

For this research, I have tried to combine the best features of the Stein and the Edell regeneration electrodes. Our electrode, like Edell's, is fabricated on silicon using standard planar microcircuit processing technology, however, we use discrete channels more on the order of the Stein electrode with the commensurate increase in selectivity and recorded signal level.

We now pause to present a mathematical model of an axon in an insulating channel with central electrodes. The derivation is paraphrased from Stein (Stein & Pearson 1971) for the unmyelinated case. Special attention is given to a problem induced by using a semiconductor substrate. In chapter 3 we shall return to the question of device structure and present the methods with which we fabricated our devices.

CHAPTER 2

In this chapter we derive the expected potentials for an axon in an insulating restricted extracellular space. As shown in figure 2-1 we measure a voltage $V_e(Z)$ within the cylindrical channel. Also shown in figure 2-1 is a configuration where we measure a voltage difference within the channel. The channel diameter is 2B, the axon diameter 2A and the channel length is L. The following derivation for the unmyelinated case* is due to Stein (Stein & Pearson 1971). Unless otherwise stated, we assume a homogeneous medium.

First we make an assumption: radial voltage drops are small compared to longitudinal voltage drops in the channel. For this to be true, $R_{e,z}$ (longitudinal extracellular fluid resistance) must be greater than $R_{e,r}$(radial extracellular fluid resistance). We know that if the extracellular fluid resistivity is ρ_e ,

---

*According to Mark and Loeb (1976), the expected voltage for a myelinated fiber is the same as that expected for an unmyelinated fiber if the channel length is at least four times the length of the internode. Usually, the internode length would be on the order of 1mm but after regeneration the node spacing is much smaller; on the order of 300um (Jacobs and Cavanagh 1969). This is suited to our purposes since we should avoid very long channels when possible.

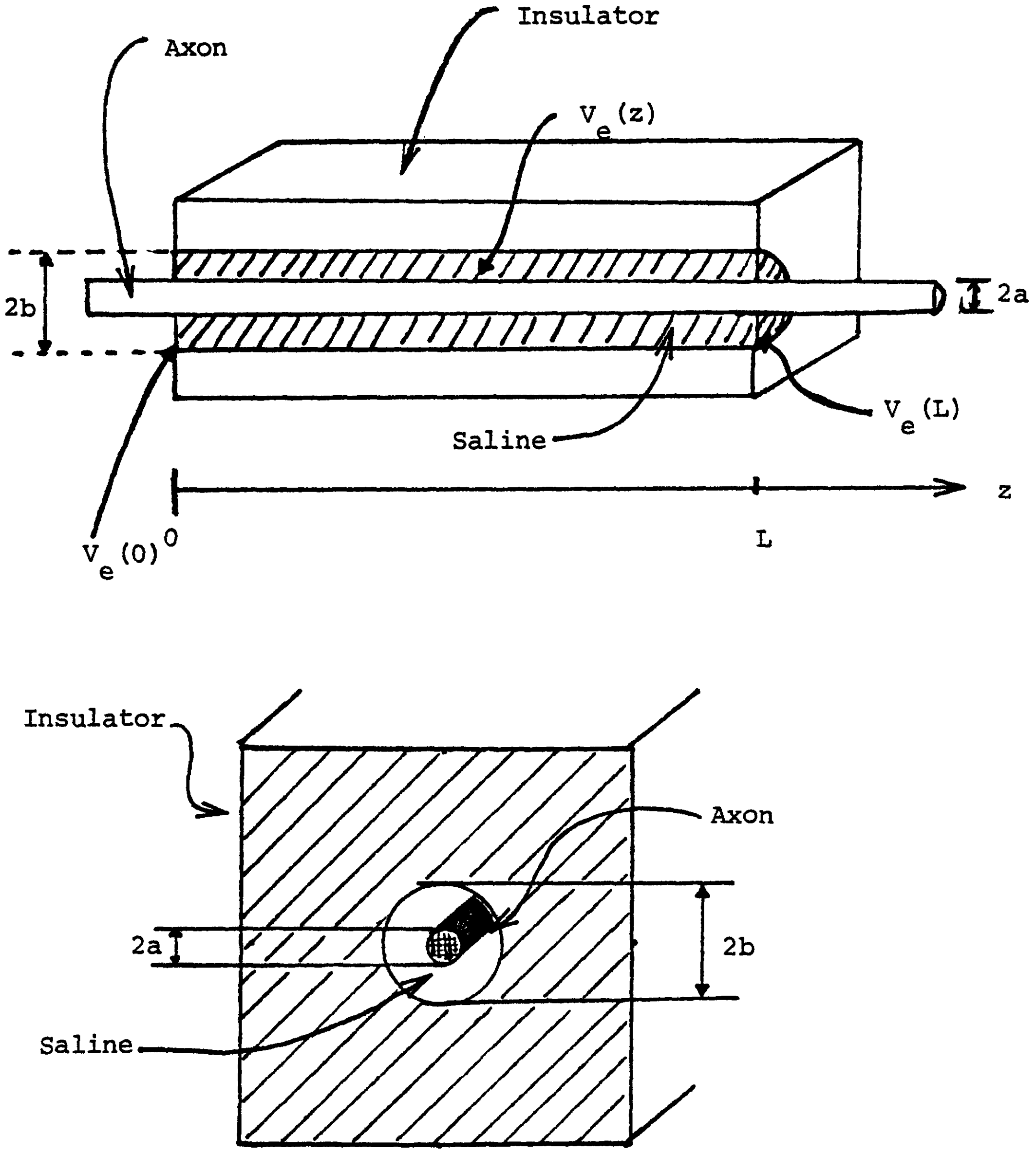

Figure 2-1a: Axon in restricted extracellular space.

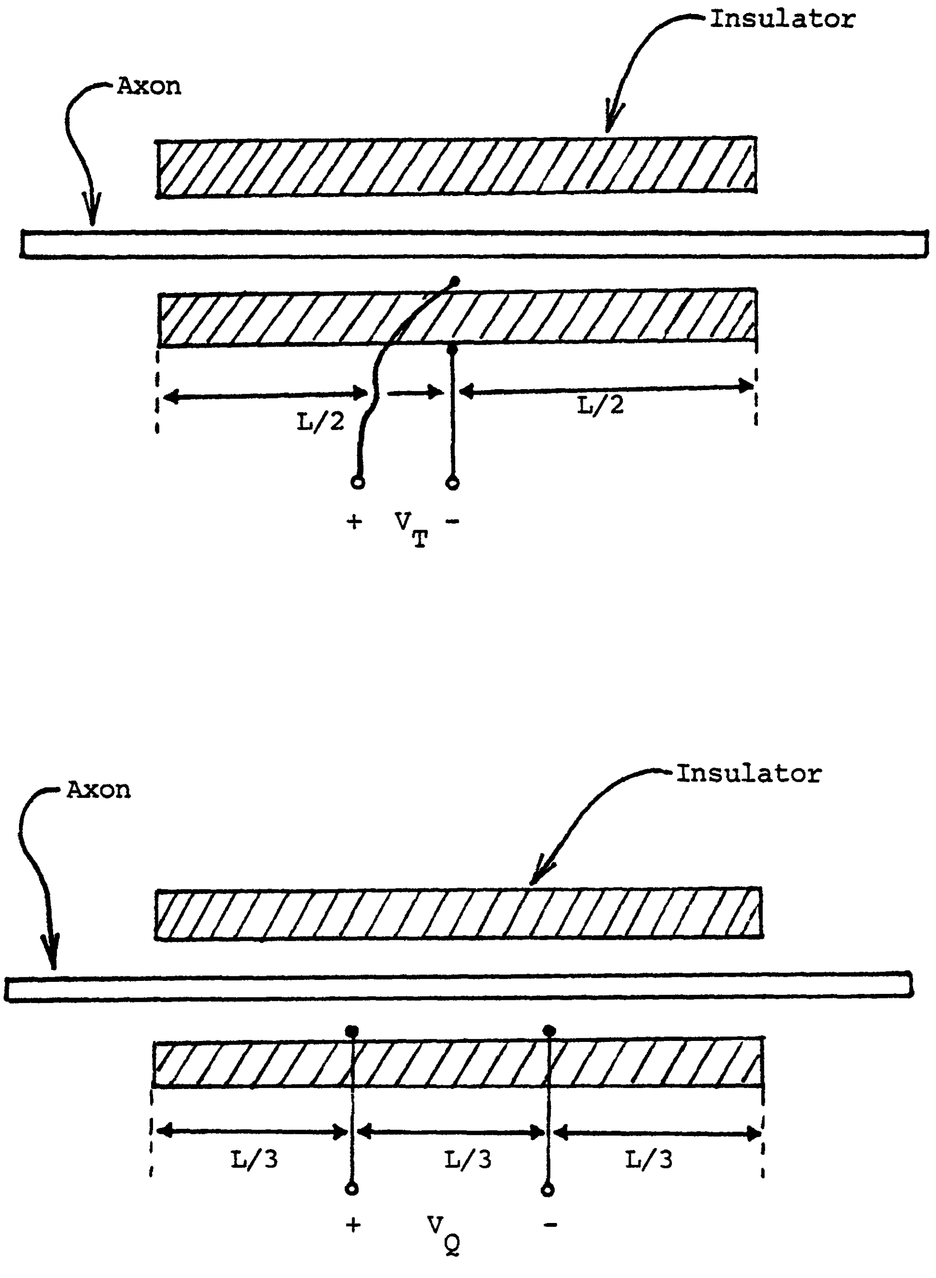

Figure 2-1b: Triphasic and Quadraphasic recording configurations.

(1) $$R_{e,z} = \rho_e L/\pi(b^2-a^2)$$

and

(2) $$R_{e,r} = (\rho_e/L)\int_a^b dr/2\pi r = \rho_e \ln(b/a)/2\pi L \quad ,$$

Thus,

(3) $$\rho_e L/\pi(b^2-a^2) \gg \rho_e \ln(b/a)/2\pi L \quad ,$$

which implies

(4) $$2L^2 \gg (b^2-a^2)\ln(b/a) \quad .$$

Assuming a channel radius of 50um, an axon radius of 2um and a channel length of 1000um we see that

$$2X10^{-6} \gg 8X10^{-9} \quad .$$

Our constraint is satisfied with a comfortable margin in theory of 10^2.

We now use the core-conductor model for unmyelinated axons and obtain the model in figure 2-2. From this model we see,

(5) $$i_m = \frac{\partial}{\partial z} i_e = -\frac{\partial}{\partial z} i_a$$

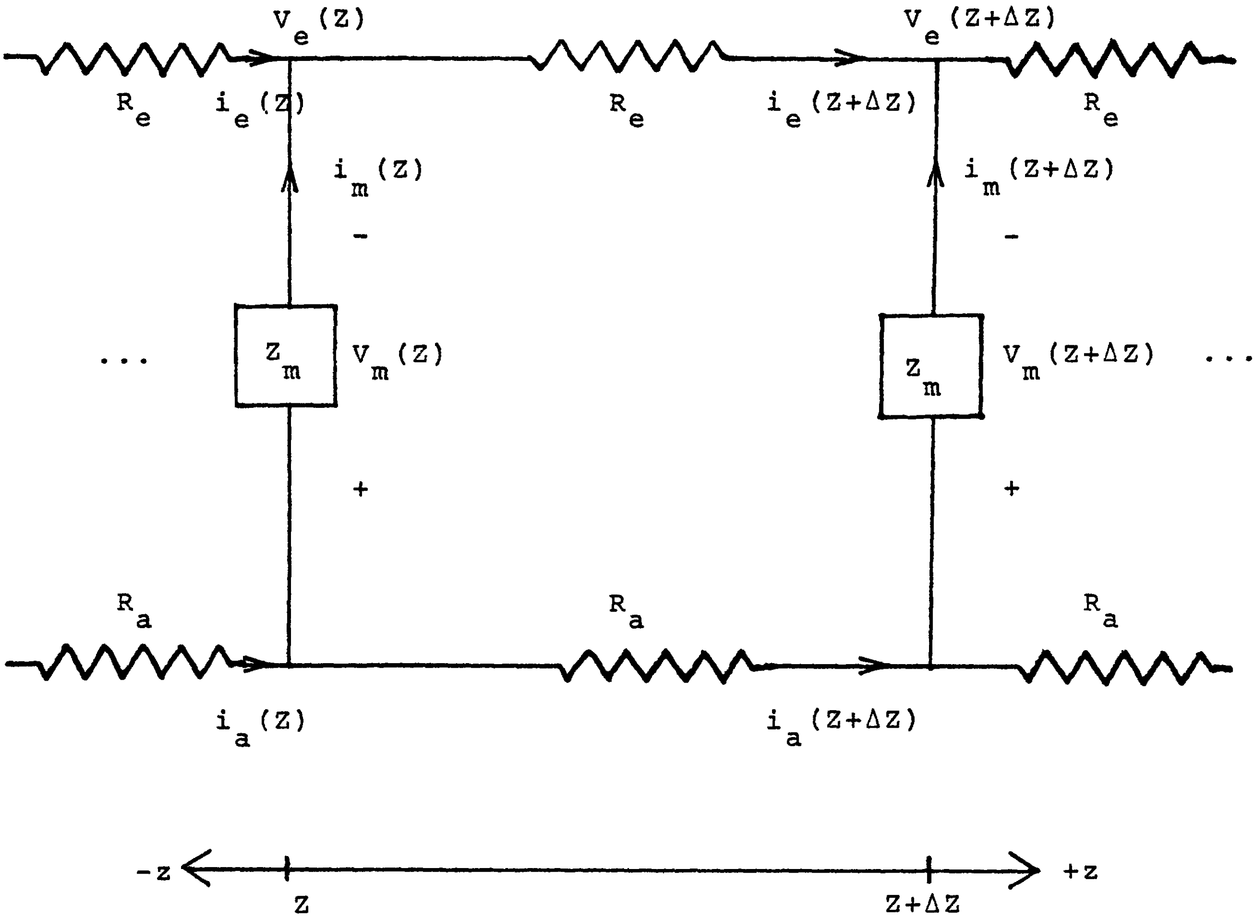

R_e - extracellular fluid resistance per unit length

R_a - axon core fluid resistance per unit length

Z_m - axon membrane impedance per unit length

i_e - longitudinal extracellular current

i_a - axon core current

i_m - axon membrane current

V_m - axon membrane voltage

V_e - extracellular voltage

Figure 2-2: Core conductor model for unmyelinated axon.

$$(6)\qquad \frac{\partial}{\partial z}V_m = R_e i_e - R_a i_a \quad .$$

We may combine (5) and (6) to show

$$(7)\qquad \frac{\partial^2}{\partial z^2}V_m = i_m(R_e+R_a) \quad .$$

We also see that in recording situation of 2-1a,

$$(8)\qquad V_e(z) = V_e(0) - \int_0^z i_e R_e dz$$

From (5) we obtain

$$(9)\qquad i_e(z) - i_e(0) = \int_0^z i_m dz \quad .$$

Substituting this into (8) we get

$$(10)\qquad V_e(z) = V_e(0) - R_e\int_0^z\int_0^z i_m dz^2 - R_e i_e(0)z \quad .$$

Combining (7) and (10)we obtain

$$(11)\qquad \begin{aligned} V_e(z) &= V_e(0)-(R_e/R_e+R_a)\int_0^z\int_0^z \frac{\partial^2}{\partial z^2}V_m dz^2 - i_e(0)R_e z \\ &= V_e(0)-(R_e/R_e+R_a)(V_m(z)-V_m(0))+Kz+C \ , \end{aligned}$$

Where K and C are lumped constants for all terms which have evolved from the integrations.

Now we seek K and C. To find them we invoke our boundary conditions at z=0 and z=L.

(12) $$V_e(z)\big|_{z=0} = V_e(0)-(R_e/R_e+R_a)(V_m(0)-V_m(0))+K\cdot 0+C\ ,$$

which implies

(13) $$C = 0\ ,$$

and

(14) $$V_e(L) = V_e(0)-(R_e/R_a+R_e)(V_m(L)-V_m(0))+KL$$

so that

(15) $$K = (\tfrac{1}{L})\left[V_e(L)-V_e(0)+(R_e/R_e+R_a)(V_m(L)-V_m(0))\right]\ .$$

Therefore,

(16) $$\begin{aligned} V_e(z) = {} & (R_e/R_e+R_a)\left[(1-\tfrac{z}{L})V_m(0)-V_m(z)+(\tfrac{z}{L})V_m(L)\right] \\ & +V_e(0)(1-\tfrac{z}{L})+V_e(L)(\tfrac{z}{L})\ . \end{aligned}$$

We now have the extracellular potential $V_e(z)$ as a function of the empirical membrane voltage $V_m(z)$ and the external endpoint voltages $V_e(0)$ and $V_e(L)$.

Consider then the voltage at mid-channel, $V_e(L/2)$ and the voltage external to the restriction located at L/2. The voltage at this external point is

$$(17) \qquad V_{out}(L/2) = \frac{1}{2}(V_e(0)-V_e(L)),$$

if we assume a homogeneous volume of saline external to our restriction. The difference between these two voltages is

$$(18) \qquad \begin{aligned} V_T &= V_e(L/2)-V_{out}(L/2) \\ &= \frac{1}{2}(R_e/R_e+R_a)(V_m(0)-2V_m(\frac{L}{2})+V_m(L)) \ . \end{aligned}$$

Let us consider a voltage difference V_Q between two points placed symmetrically in the restricted channel,ie;

$$(19) \qquad V_Q = V_e(L/3)-V_e(2L/3),$$

as illustrated in 2-1b.

If we assume a large volume of saline external to the restriction, then $V_e(0)$ is approximately equal to $V_e(L)$ so that

$$(20) \qquad V_Q = \frac{1}{3}(R_e/R_e+R_a)(V_m(0)-3V_m(\frac{L}{3})+3V_m(\frac{2L}{3})-V_m(L))$$

Now we examine the behavior of V_T and V_Q for the length L small relative to the wavelength of the propagating action potential $V_m(z,t)$. Assuming constant speed of propagation, c, we have

$$(21) \qquad V_m(z,t) = V_m(t-\frac{z}{c})$$

This transforms (18) and (20) into

$$(22) \qquad V_T(t) = \frac{1}{2}(R_e/R_e+R_a)(V_m(t-\frac{L}{2c})-2V_m(t)+V_m(t+\frac{L}{2c}))$$

and

$$(23) \qquad V_Q(t) = \frac{1}{3}(R_e/R_e+R_a)(V_m(t-\frac{L}{3c})-3V_m(t)+3V_m(t+\frac{L}{3c}) -V_m(t+\frac{2L}{3c})) \quad .$$

If we remember that

$$(24) \qquad \frac{d^2}{dx^2}f(x) = \lim_{\Delta x\to 0} \frac{f(x-\Delta x)-2f(x)+f(x+\Delta x)}{\Delta x^2}$$

and

$$(25) \qquad \frac{d^3}{dx^3}f(x) = \lim_{\Delta x\to 0} \frac{f(x-\Delta x)-3f(x)+3f(x+\Delta x)-f(x+2\Delta x)}{\Delta x^3}$$

we see that if L is small relative the wavelength of the action potential,

$$(26) \qquad V_T(t) \simeq \frac{1}{2}(R_e/R_e+R_a)(L/2c)^2\frac{\partial^2}{\partial t^2}V_m(t)$$

$$(27) \qquad V_Q(t) \simeq \frac{1}{3}(R_e/R_e+R_a)(L/3c)^3\frac{\partial^3}{\partial t^3}V_m(t)$$

Another expression which will be useful is one which is visibly dependent on the channel geometry. R_e and R_a are given by

$$(28) \qquad R_e = \rho_e/\pi(b^2-a^2)$$

$$(29) \qquad R_a = \rho_a/\pi a^2$$

where ρ_e and ρ_a are the resistivities of the fluid in the extracellular and intracellular space respectively. For unmyelinated squid axon $\rho_e \simeq \rho_a/2$* so that

$$(30) \qquad R_e/R_e+R_a \simeq 1/(1+(b^2-a^2)/2a^2)$$

---

*These resistivities were calculated from external and axoplasmic concentrations and diffusivities of Na^+, K^+, and Cl^- in squid. The actual ratio of $\rho_e/\rho_a = 2/3$ was taken to be 1/2.

For the radius of the axon small relative the radius of the channel but not so small that (4) is violated we have

$$(31) \qquad R_e/R_e+R_a \approx 2(a/b)^2$$

Combining (31) with (26) and (27) we have

$$(32) \qquad V_T(t) \approx (\frac{L}{D})^2 (\frac{a}{c})^2 \frac{\partial^2}{\partial t^2} V_m(t)$$

$$(33) \qquad V_Q(t) \approx \frac{1}{10}(\frac{L^3}{D^2})(a^2/c^3)\frac{\partial^3}{\partial t^3} V_m(t)$$

where D is the diameter of the channel and L is the channel length.

It would be advisable to obtain peak values for $V_T(t)$ and $V_Q(t)$ so as to know what signal level can be expected for our two electrode configurations.

A typical action potential wavefrom is shown in figure 2.3 (Cole 1968). A discrete waveform was obtained by sampling this trace. The first, second, and third differences were computed. Before each difference operation, the discrete valued waveform was smoothed using a low pass digital filter. This was done to avoid differentiating the high frequency observation noise introduced by visually sampling the continuous waveform. This filtering also induced low amplitude error oscillations in trailing parts of the difference but these occur in a region of little interest to us so we ignore them.

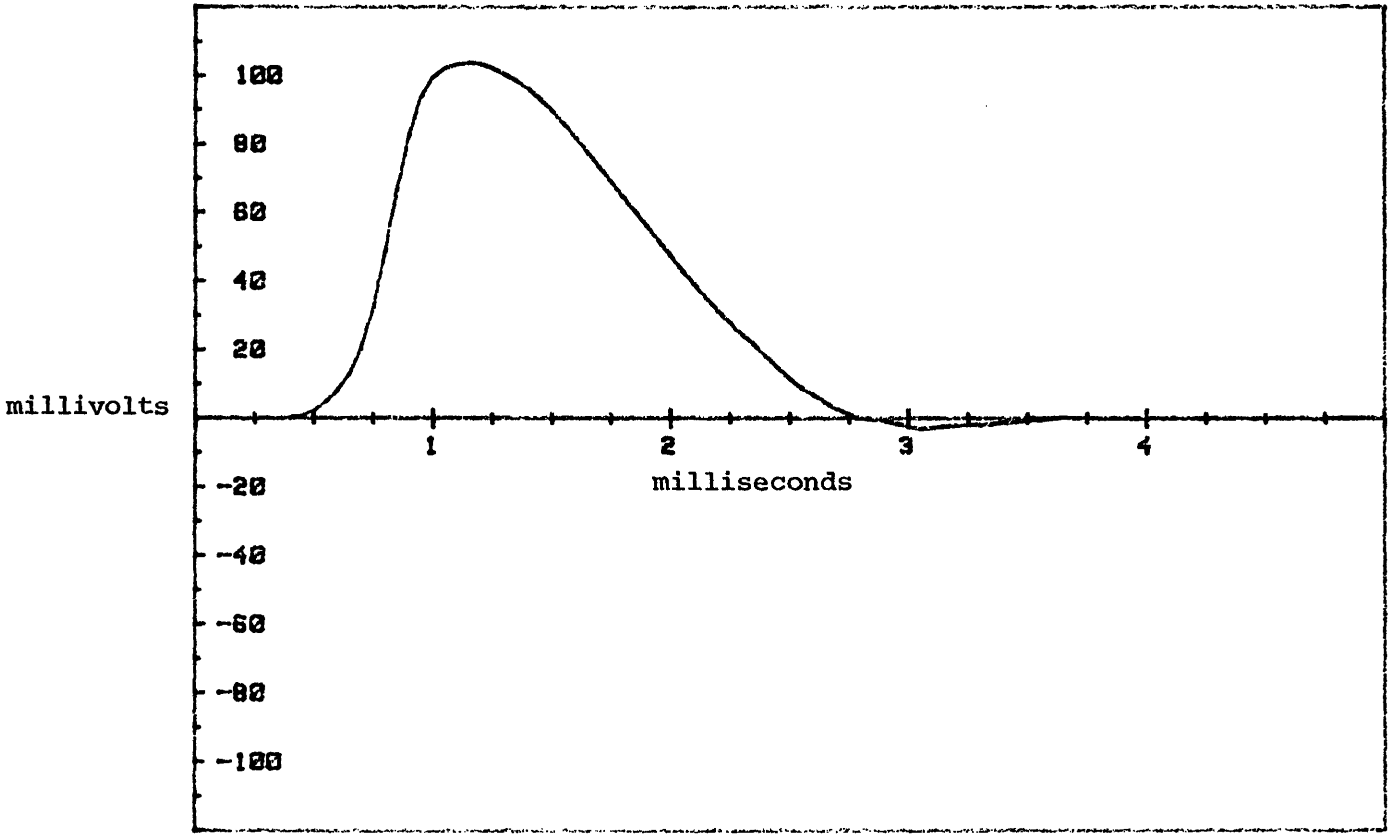

Figure 2-3: Typical action potential waveform (Cole 1968).

The differences computed by this method are shown in figure 2.4. From these we may obtain peak to peak values for $V_T(t)$ and $V_Q(t)$. Notice that the second difference is triphasic and the third difference (V_Q) is quadraphasic. For this reason the subscripts Q and T were chosen.

From figure 2.4 we have $\frac{\partial^2}{\partial t^2}V_{mp-p} = 3.6\mathrm{x}10^6$volt/sec^2 and $\frac{\partial^3}{\partial t^3}V_{mp-p} = 3.6\mathrm{x}10^{10}$volt/sec^3. In myelinated amphibian fibers a typical diameter to conduction velocity ratio is 5um/10m/s = 5x10^{-7}sec (Bullock & Horridge 1965). This yields, using equations (32) and (33).

$$V_{Tp-p} = (L/D)^2(1.3\mathrm{uV}) \tag{34}$$

$$V_{Qp-p} = (L^3/D^2)(1.3\mathrm{X}10^{-4}\mathrm{uV/um}) \tag{35}$$

For a channel length of 1000um and a diameter of 50um, these yield peak values of 520uv and 51.2uv for V_T and V_Q respectively.

Until now we have assumed a purely insulating restricted extracellular space. A semiconductor insulated by oxide or nitride is to be the channel material, since ultimately we would like to put amplifying and addressing circuitry at the recording site. Here we encounter a potential problem. The resistivity of most lightly doped semiconductors is much smaller than the resistivity of the extracellular saline (1 ohm-cm versus 100ohm-cm). The semiconductor, relative the saline, is an ideal conductor. Thus our structure intro-

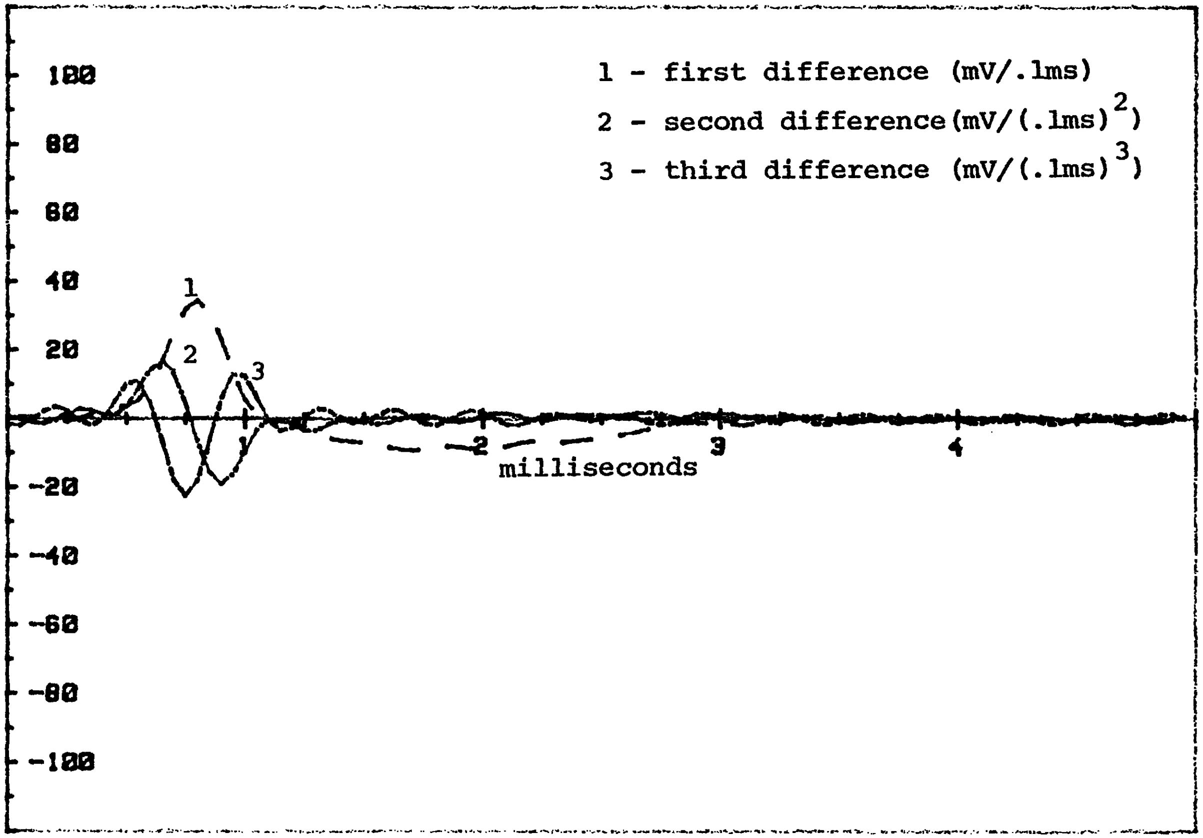

Figure 2-4: First second and third differences for sampled action potential.

duces a parasitic Saline-Oxide-Semiconductor (SOS) capacitance. Figure2-5 shows the physical arrangement and an equivalent circuit model for an unmyelinated axon in a SOS channel.

About any node to which C_p, our parasitic capacitance, is attached we have by Kirchoff's current law,

$$\frac{\partial}{\partial t} i_e = i_m - i_p \quad . \tag{36}$$

If i_p, the parasitic current, is on the order i_m, the membrane current, then its effect will be noticeable. Let us investigate further. We see that

$$i_m = V_m/R_m + \frac{\partial}{\partial t} V_m C_m \tag{37}$$

and

$$i_p = \frac{\partial}{\partial t} V_e C_p \quad . \tag{38}$$

As before, let the channel length be 1000um and the diameter 50um. From our difference curves we see that $\frac{\partial}{\partial t} V_m$ has a peak to peak value of approximately 430 volts/second whereas $\frac{\partial}{\partial t} V_{Tp\text{-}p}$ is only 5 volts/second.

Now let us look to the actual values of C_m and C_p.

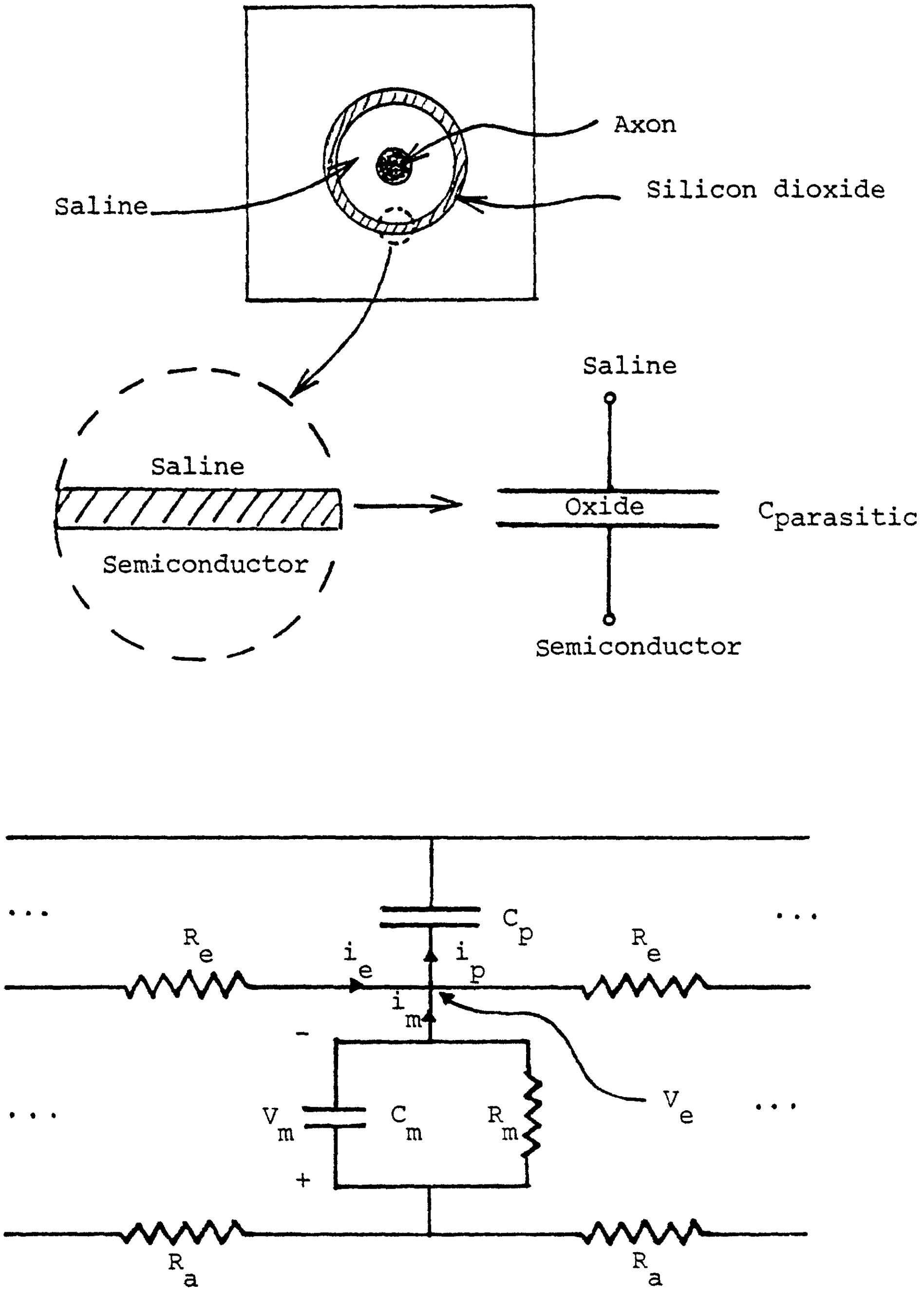

Figure 2-5: Unmyelinated axon in a Saline-Oxide-Semiconductor channel, and equivalent circuit model.

The axonal membrane capacitance is roughly 2uF/cm^2 for unmyelinated fibers and the node of myelinated fibers. The capacitance of the internode of myelinated fibers is 5000pF/cm^2 (Florey 1966)*. For an oxide thickness of 1um the capacitance is 3451pF/cm^2. Assume a small unmyelinated fiber of diameter 1um* and again a channel diameter of 50um. The capacitance per unit length C_m must be 628pf/cm and C_p must be 54.2pF/cm. C_m is substantially larger than C_p even for the smaller unmyelinated fibers. Couple this with the large amplitude of $\frac{\partial}{\partial t}V_m$ relative $\frac{\partial}{\partial t}V_e$ and readily see that $i_p << i_m$. Therefore, the parasitic effects of C_p are negligible in unmyelinated axons.

For myelinated axons, the same argument is valid at a node of ranvier, but we must also examine the internode. A circuit model appears in figure 2-6. C_p will be as before since it is determined by channel dimensions. Taking a small myelinated axon of diameter 4um*, we have $C_{my} = 6.28$pF/cm. C_{my} is approximately nine times smaller than $C_p = 54.2$pF/cm. We still have $\frac{\partial}{\partial t}V_m$ greater than $\frac{\partial}{\partial t}V_e$ by a factor of ninety, however. This will leave i_{my} greater than i_p by a factor of ten. Thus, for myelinated axons as well as for unmyelinated axons, the effect of the SOS parasitic capacitor is theoretically negligible even for the smallest fibers.

---

*in amphibia

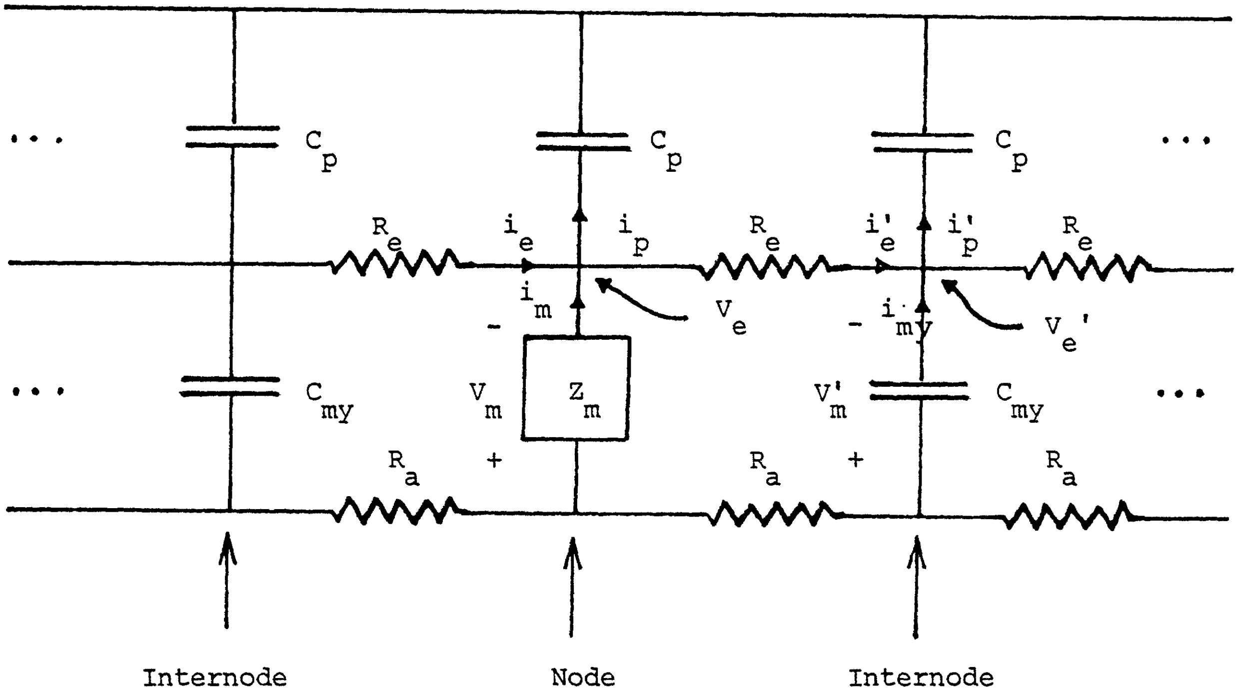

Figure 2-6: Myelinated axon in a SOS channel; circuit model.

Even if this proves false empirically, we are still not outdone since thicker oxide layers may be used thereby depressing the capacitance C_p**. In short, C_p will not interfere with our measurements.

With the theoretical considerations now explored we may proceed to the design of our device in Chapter 3.

**If necessary, thick oxide layers may be applied by sputtering techniques since thermally grown oxides are unfeasible for thicknesses greater than 2um.

CHAPTER 3

When assigned the task of designing any implant for use in living animals, we are confronted by a dual problem. The implant must be able to perform its designated tasks as well as remain inert to the hostile internal environment of the organism.

In our endeavor to incorporate microelectronic technology in our recording/stimulating instrument we note the seemingly complete incompatability of biological systems and semiconductor devices. Though silicon and silicon dioxide are relatively inert in a physiological setting, arsenic, phosphorous and boron, three of the principal dopants used, are poisonous. Sodium is abundant in physiological fluids. It is also very mobile in silicon dioxide and contributes to device degradation; especially in field effect transistors where mobile oxide charge changes the threshold of the device. In addition, biological systems, especially mammals, are relentless in their attempts to break down foreign bodies. Silicon dioxide is inert, but only to a point. In chronic applications, the thin layer of SiO_2 used in passivation may degrade. Thus, we see that our device could poison the animal and likewise, the animal could poison our device.

One of these problems disappears upon closer inspection and the other is solvable. Very low dopant concentrations are used (typically one part in 10^8) and it is unlikely that these dopants would diffuse out of the silicon substrate in any appreciable quantities since their diffusivities at physiological temperatures are very low. If the device is encased in silicon nitride*, except for the noble metal electrode faces, it will be hermetically sealed, thereby solving the problem of keeping the inside in and the outside out. We now see that silicon based microcircuitry and biological systems are not as incompatible as first imagined.

As seen in Chapter 2, the voltages V_T and V_Q are both small, however, V_T is larger than V_Q by a factor of ten, so let us consider only the triphasic recording. In such a recording situation we would have an insulating channel with a central electrode as shown schematically in figure 3-1. The problem is to pack many such channels as densely as possible in a silicon substrate. Electrical contacts would be run from the central electrodes to footpads. To the footpads, transcutaneous insulated wires would be connected. A polymer guide cuff to assure regeneration through our channels would be attached to the device and the regeneration electrode would be complete. This concept is illustrated in figure 3-2.

Several approaches to the implementation of this concept were considered. The final method, that of polymer ridges

---

*For this thesis, thermal oxide was used exclusively, and no nitride layer was deposited, the reason being that there was no available means to do this in our laboratory. Also, the devices presented herein were not to be chronically implanted. Thus, the introduction of nitride passivation was not crucial.

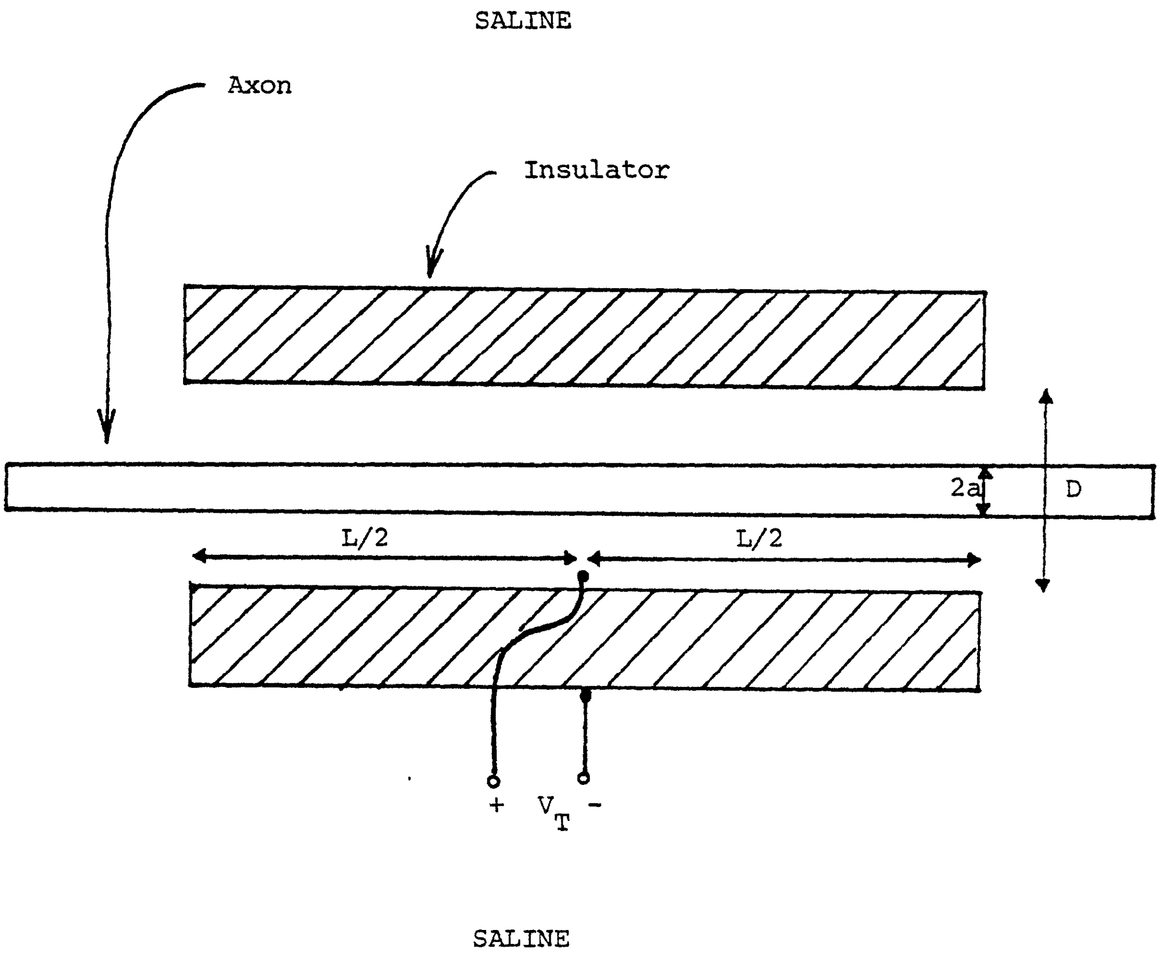

Figure 3-1: Triphasic recording; central electrode.

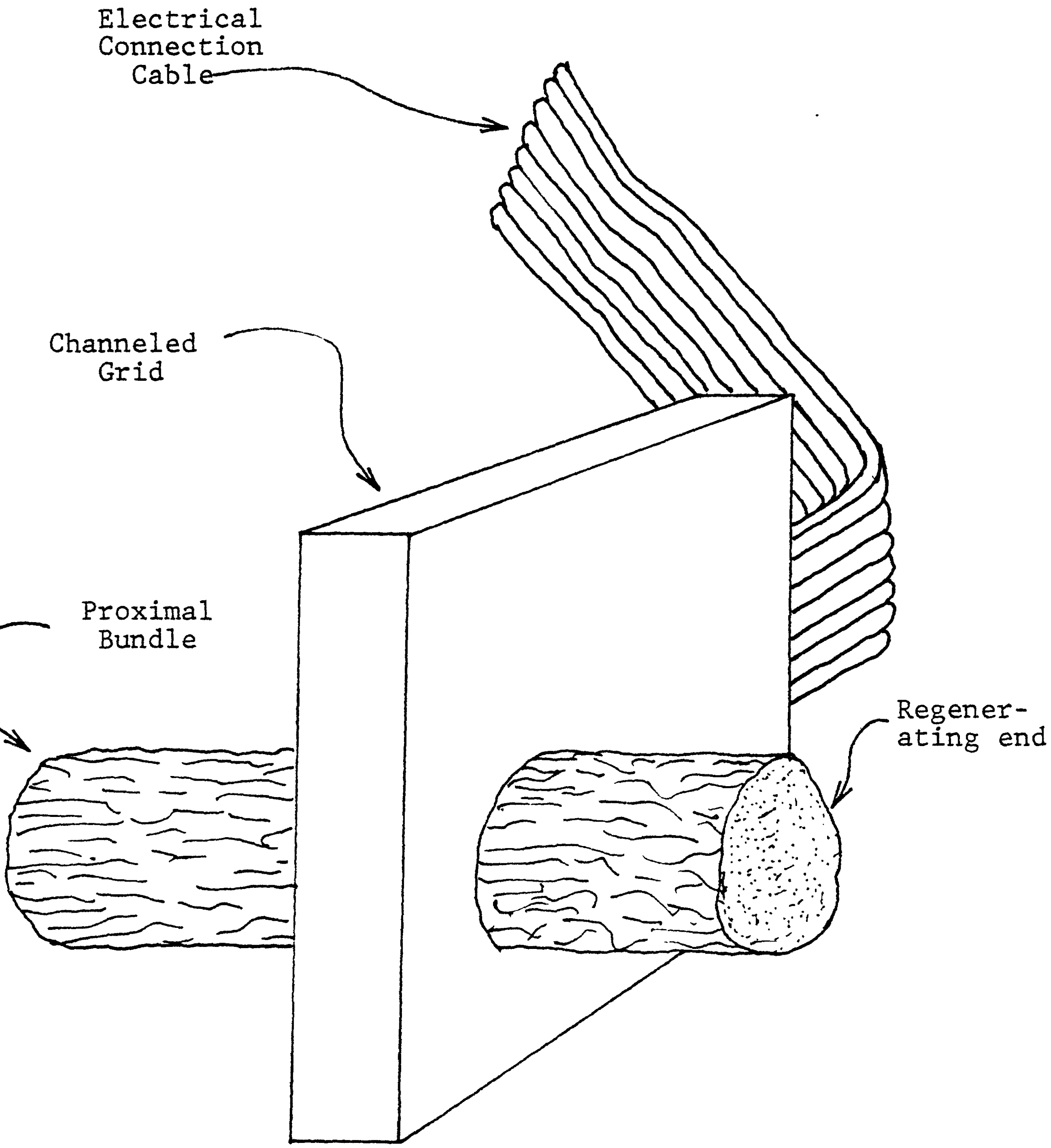

Figure 3-2: Concept of the regeneration electrode.

forming channels on a planar silicon circuit, is an end result reached by a series of refinements and compromises.

Initially, a larger scale implementation of one of the techniques used by Mannard & Stein (1974) was considered wherein thin metal wires were embedded in epoxy and later etched to leave channels in the epoxy of the proper dimensions. It was reasoned that if an epoxy boule with precisely embedded wires could be made, then wafers with preformed channels could be cut and polished. Using such wafers we could either lay metal electrode patterns on the surface using standard photolithographic techniques, or lay an epilayer of silicon on the epoxy from which we could fabricate microcircuitry. An unprocessed wafer from the same boule would then be place atop the processed wafer, aligned and bonded, resulting in channels with central electrodes. Figure 3-3 depicts the envisioned process steps. This method was abandoned, however, due to technical difficulties foreseen in making the epoxy boule.

Next, machining holes in silicon wafers with a laser was explored. Using an X-Y micromanipulator, standard glass optics, and a high power N-YAG laser, frequency doubled to 560mm, grids of small holes were put in 250um thick silicon wafers. The entrance holes on the backside of the wafer were 75um in diameter and the exit holes on the polished face were approximately 25um in diameter. The front and backside of one grid are shown in figure 3-4a and 3-4b respectively. The wafer was then cleaned and oxidized. A metal electrode pattern was

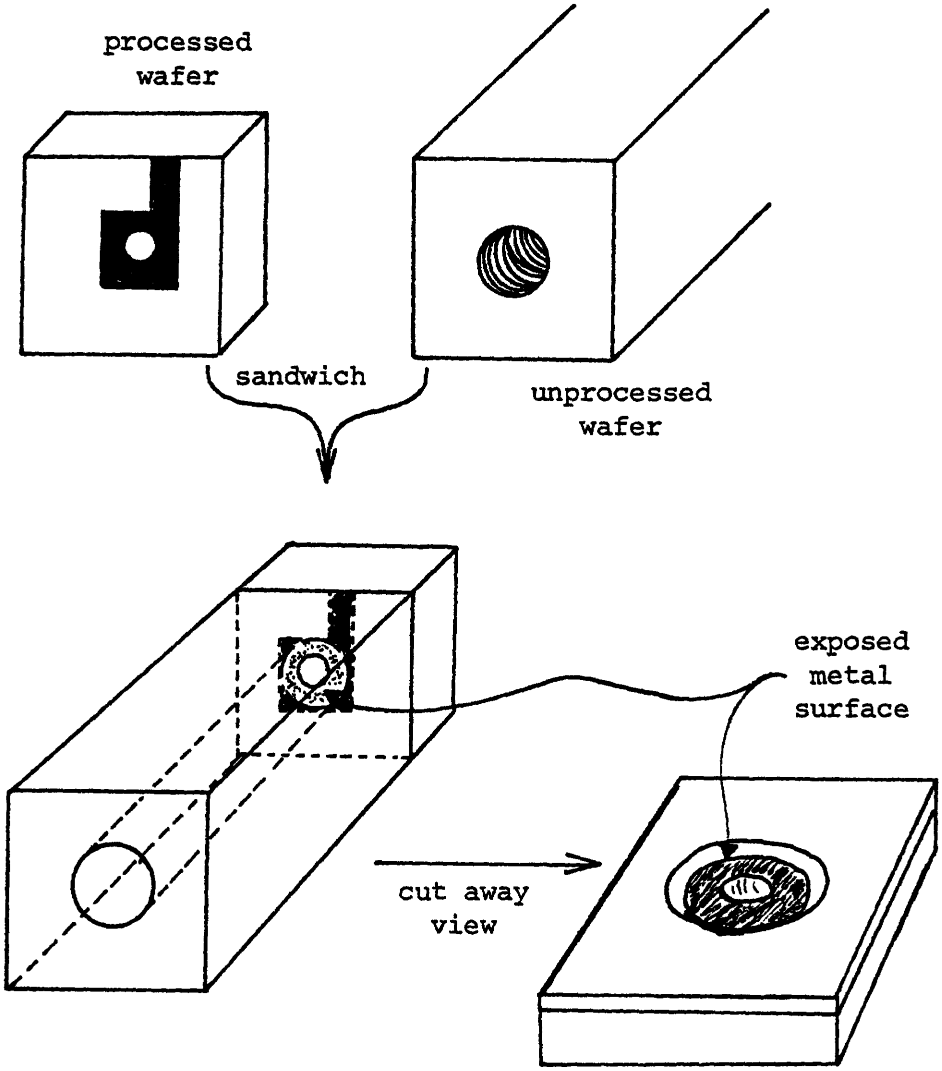

Figure 3-3: Envisioned process steps using epoxy boule (see text).

formed over the grid (figure 3-4c) and then sandwiched by a piece of mylar* containing a similar grid with slightly larger holes (figure 3-4d).

The resulting structure was very much like the original concept, however, it suffered some flaws. By its very nature, laser milling is a highly traumatic process. Since the material in the path of the focused laser beam is vaporized upon exposure, hole drilling is accomplished in a series of small explosions. What this does to the silicon crystal lattice was not studied, but there is a chance that the lattice is disrupted. This would be disastrous for silicon circuitry near the hole. Another flaw involved the time and effort needed to drill a grid of holes. Each hole took approximately fifteen seconds to drill using the maximum power allowable to avoid wafer surface fracture. Though the beam positioning could be computer controlled ultimately, the process would not be suited to batch processing and thus undesirable. Couple these problems with the fact that a mylar cover grid would have to be optically aligned, and the fact that the length to diameter aspect ratio of the holes is limited by lens quality and beam divergence, and we see that in the long run, this processing scheme would be both size limited and costly. Therefore, we seek a more tractable process. At this point it was decided to use a more standard microstructure fabrication technology rather than forge a new path.

---

*A thermosetting adhesive was placed (Bostik 10-250-2) on the face of the mylar wafer abutting the silicon before laser machining to expedite bonding to the silicon.

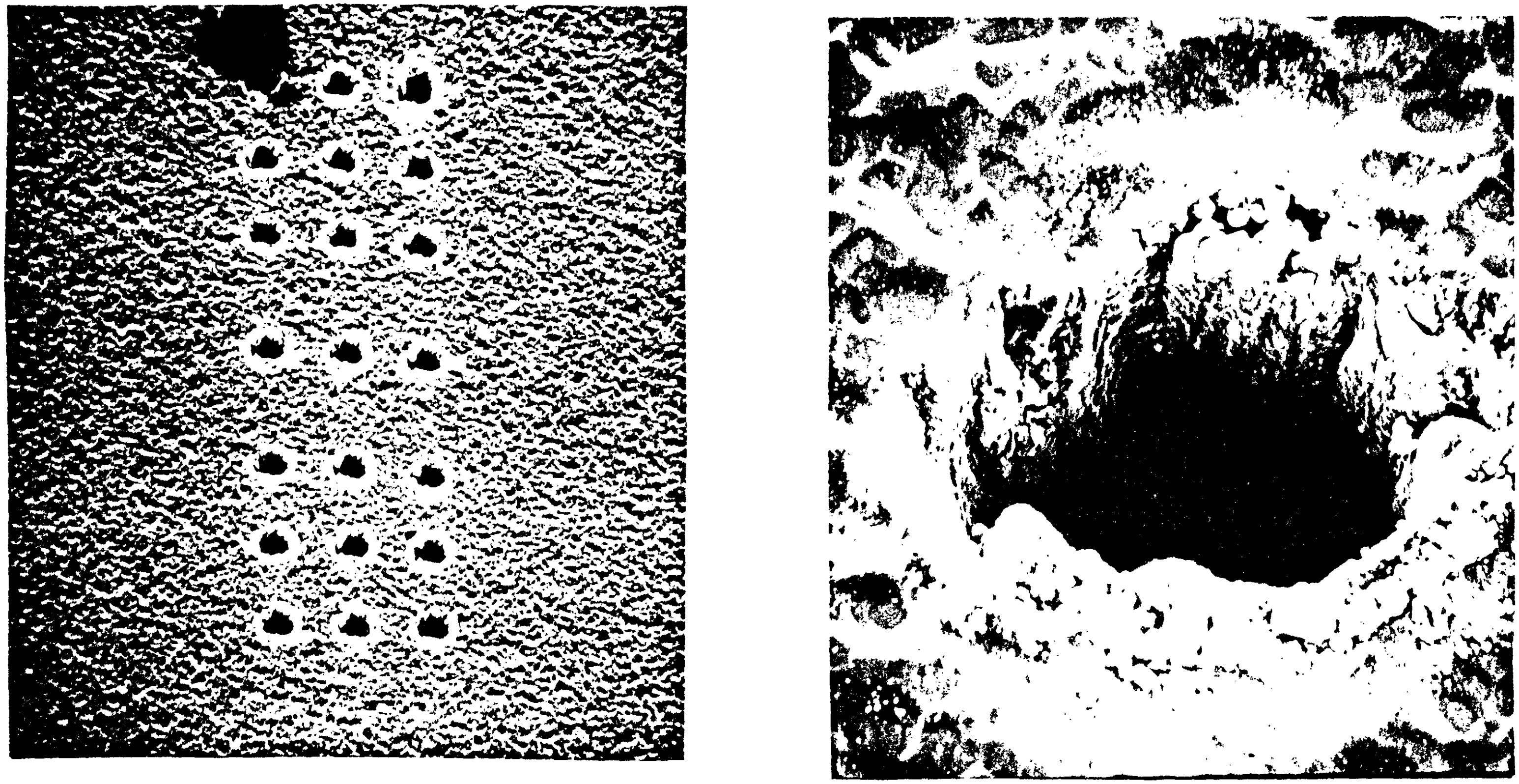

40X

1000X

Figure 3-4a: Laser milled entrance holes in silicon (backside)

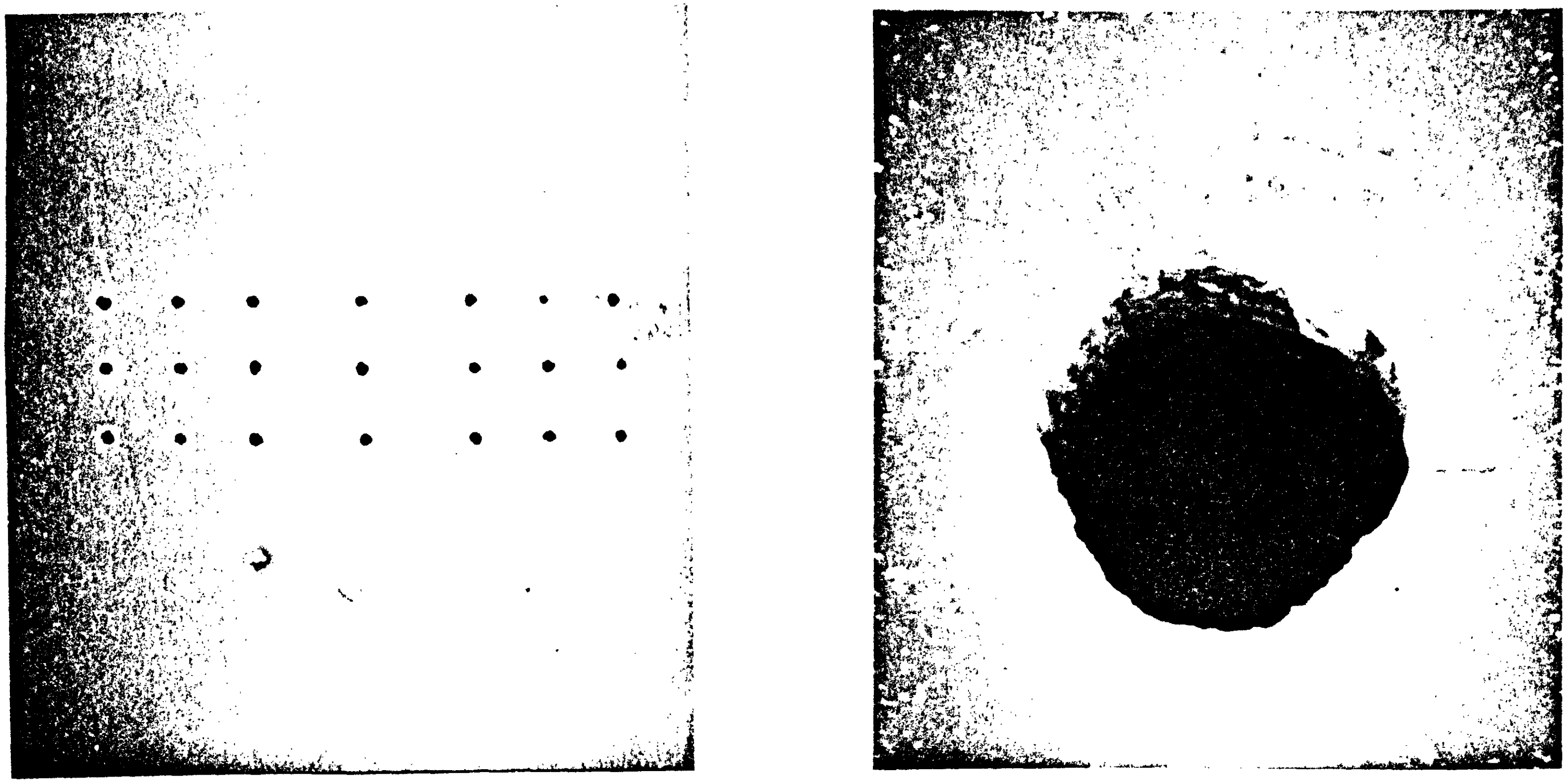

40X

2000X

Figure 3-4b: Laser milled exit holes in silicon (polished side).

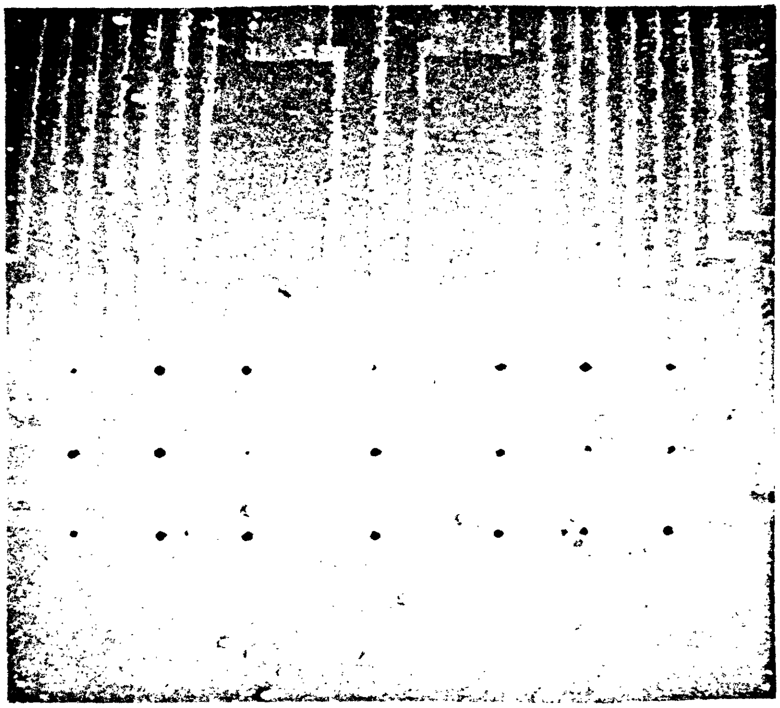

Figure 3-4c: Grid of holes with poorly etched metal electrode pattern.

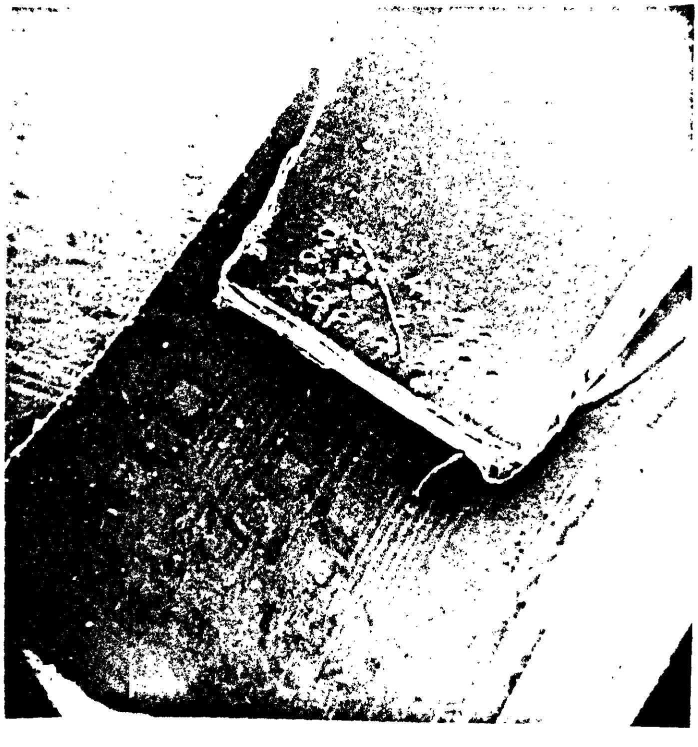

Figure 3-4d: Grid in silicon covered with similar grid in mylar.

It is possible with a properly aligned mask to anisotropically etch moats on the surface of the silicon wafers with certain crystalographic orientations (Bean 1978, Bassous 1978). Specifically, wafers with a (100) surface orientation may produce self-limiting triangular moats (figure 3-5) and wafers with (110) surface orientation may produce vertical sidewall moats of arbitrary depth (figure 3-6). The etchant used is 35% KOH in $H_2 0$ by weight at 80^oC. We will dispense with the actual mechanics of the process and refer the interested reader to Bassous (1978) and Bean (1978).

If we etch many long parallel moats of the proper width (say 50um) and cover them, we have produced isolated channels in silicon. If a recording electrode is placed in the center of each channel, we have a slightly compromised version of our original idea (figure 3-7a) It is compromised in the sense that the channels lie in one line rather than distributed over a two dimensional cross-section as are nerve bundles. However, this is not too bad a compromise since such devices could be stacked (figure 3-7b) and though the minimum vertical channel separation we can achieve is indeed limited by this method*, the horizontal separation and channel width may be controlled to submicrometer dimensions (Bean 1978). Since as previously discussed, most axons do not have submicrometer diameters, we are virtually unlimited by processing constraints in the horizontal direction.

---

*Handling wafers thinner than 150um is unfeasible at present.

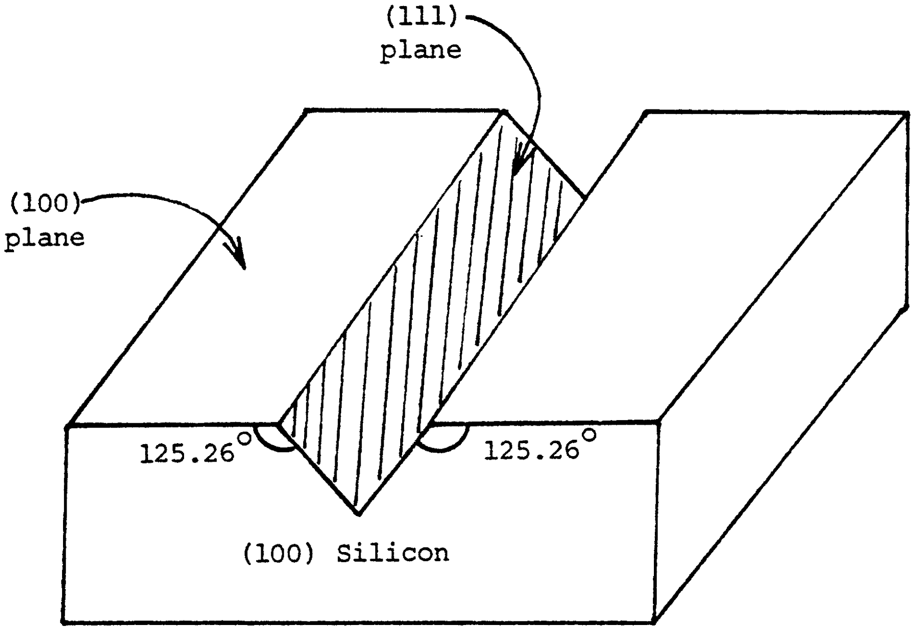

Figure 3-5: Triangular moat anisotropically etched in (100) Silicon.

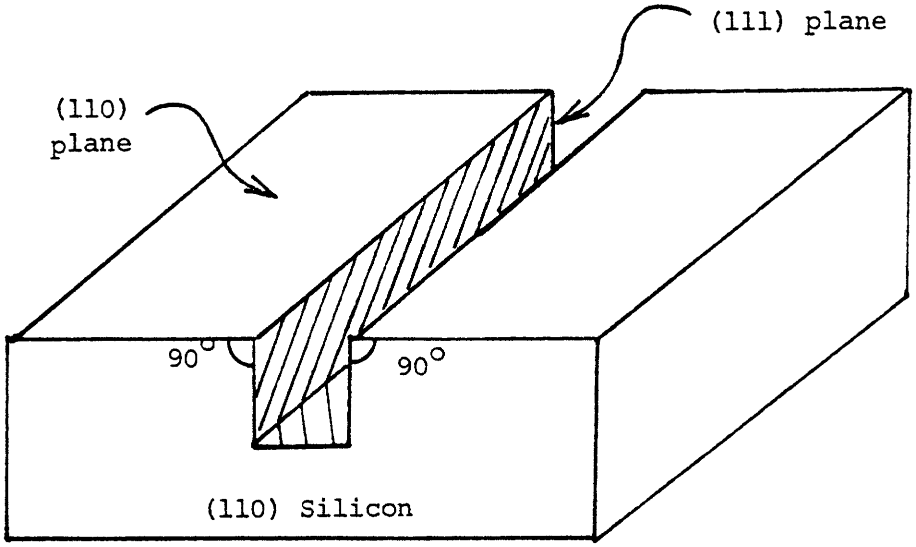

Figure 3-6: Vertical sidewall moat anisotropically etched in (110) Silicon.

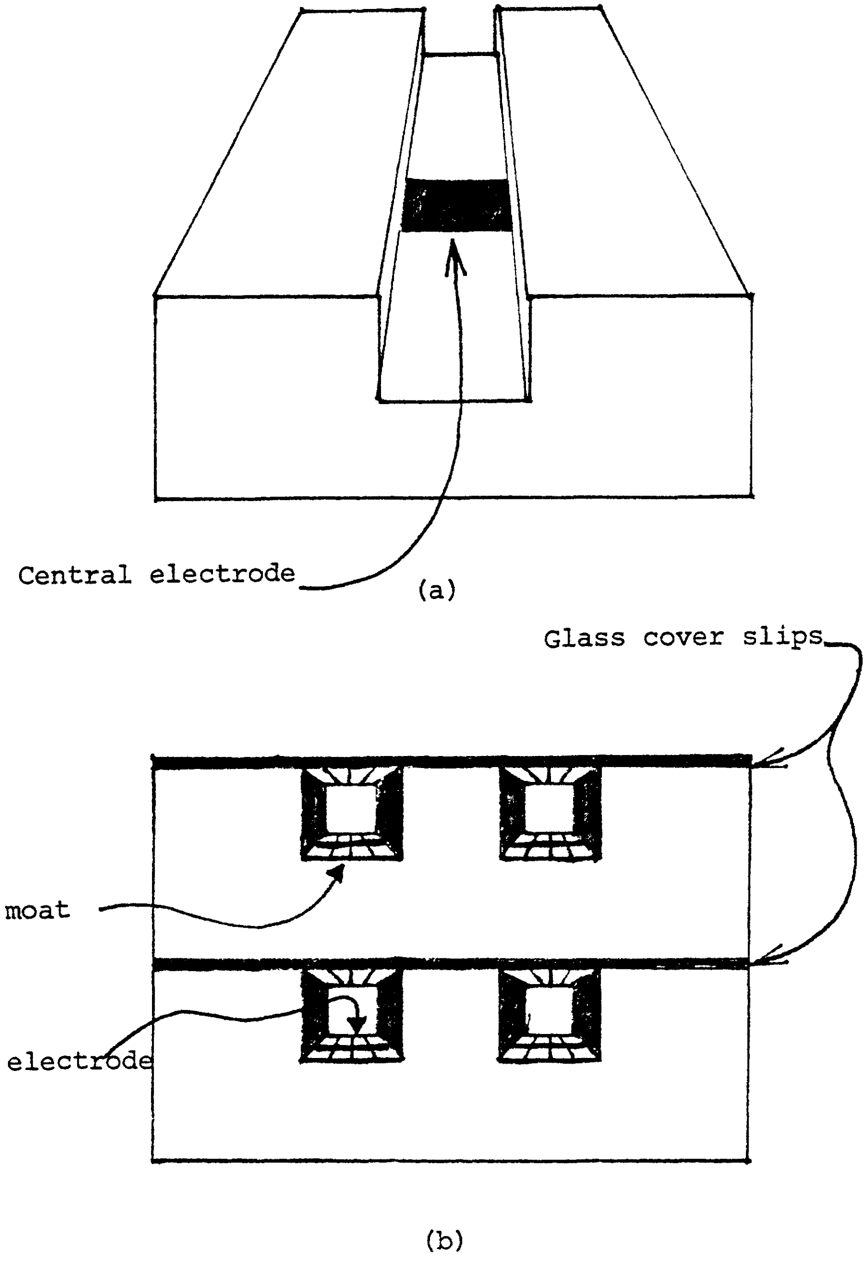

Figure 3-7: (a) Moat with central electrode. (b) Stacked moats.

We still have a problem, however. Current photolithographic techniques rely upon contact printing. If a moat is 50um deep, will it be possible to pattern the bottom since we cannot actually come into contact with it? Will the penumbra induced by the 50um offset and our imperfectly collimated beam give resolution so poor that features in the moat bottoms will bleed into each other, or fail to register?

For the system in our lab, the exposure beam on the mask aligner was well collimated and gave a penumbra of only 5um for a mask offset of 75um. Thus, we have a penumbra to offset ratio of 1/15. This is usable if we avoid line widths of less than 10um in 75um moats.

Yet another problem arose. The preceding argument is predicated upon having a thin even film of photoresist over the entire wafer surface; including the moat bottoms. After trying a variety of application techniques, including both dipping and spinning with various viscosity resists (Kodak KTFR, Shipley 1350B and J) it was found that one of two things occurred. Either the ridges between the moats were devoid of photoresist and the moat bottoms were thinly and evenly coated, or the moat bottoms were thickly covered and the ridges had thin and even coats. No happy medium could be reached, so patterning the moats with photoresist was abandoned. The case is by no means closed, however, since there may be some means of applying photoresist to such microstructures. Qualitatively, the problem seems to be that low viscosity resists, though they do not plug the moat bottoms, have too little adhesion and toomuch surface tension to adhere to the ridges whereas higher viscosity resists overcome the surface tension and adhere well only to be overzealous in this respect on the moat bottom. A low viscosity resist with ultralow surface tension and excellent SiO_2 adhesion would seem to be indicated, but that problem lies beyond the scope of this thesis.

If we modify our design slightly we may avoid having to pattern moat bottoms. In a finished device, the moats will be covered to create channels, so if instead of putting the circuitry in the moat, we construct it on a planar substrate and then align the circuit over the moats, we again have a channel with a central electrode. Figure 3-8 illustrates this concept. Unfortunately, moat alignment is a must in this process, and we would do well not to avoid this feature. Also, fastening the moat structure to the planar circuitry might prove difficult especially since we must avoid unwanted adhesive on the electrode faces which would render them inoperative. For these two reasons, this method was not fully explored, but it does remain a possible option*.

We come now to the processing technique with which our devices were fabricated. The basic idea is very simple. After an electrode has been laid on a planar surface, channel walls are placed around it. The result as before is a moat with an electrode on its bottom (figure 3-9). The difference is

---

*PSG bonding (Bassous 1978) and electrostatic bonding (Shapiro and Terry 19798) were not explored.

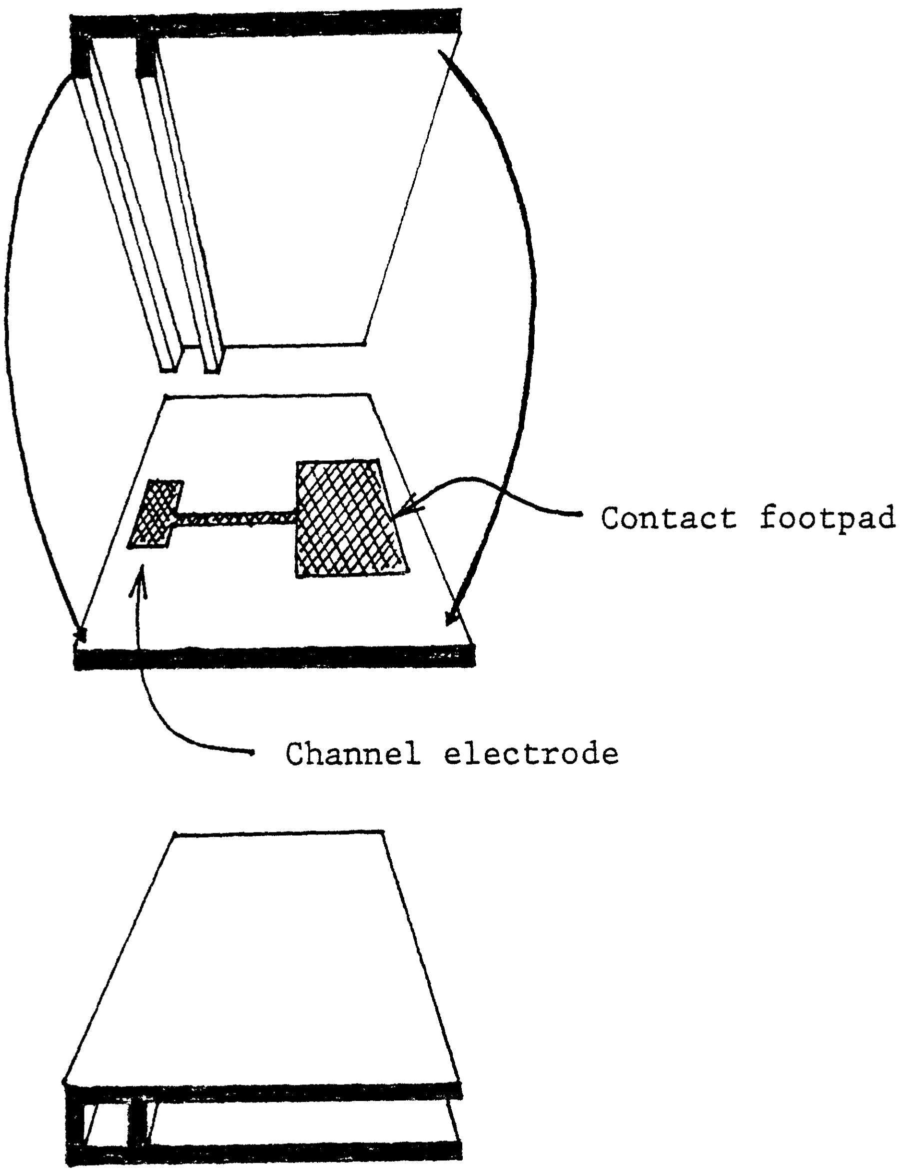

Figure 3-8: Planar electrode pattern aligned with moat walls to create electrode channel.

that we have used only standard planar techniques.

Using reactive ion etching, aluminum masks, and a polymer called Polyimide (DuPont), such channel walls may be placed on a silicon substrate with submicrometer dimensions (DeGraff and Flanders 1979). This technology is a result of the efforts of the Microstructure Laboratory of M.I.T. to make zone plates for x-ray diffraction. The etching takes place in a low pressure oxygen atmosphere and gives a highly directional etch. 35um high, 1um wide ridges have been obtained with this technique. Polyimide is also very inert and therefore most toxicity fears should be allayed.

Our general procedure will be to 1) create a multi-electrode pattern on a planar silicon substrate, 2) cover the substrate with an appropriate thickness of polyimide, 3) lay a channel wall mask pattern in aluminum atop the polyimide aligned to the underlying electrodes, 4) reactive ion etch the unwanted polyimide and 5) remove the residual aluminum of the channel mask. We may now concentrate on the design of the planar electrode array. A transcutaneous connection cable will be considered later.

Another application of this technology is also possible. Since application of polyimide to an irregular surface tends to planarize the surface, we could imagine applying the polymer to our previously mentioned moats of figure 3-5. An aluminum pattern could then be laid atop the polyimide and we could vertically etch down to the substrate. This would form a mask with the

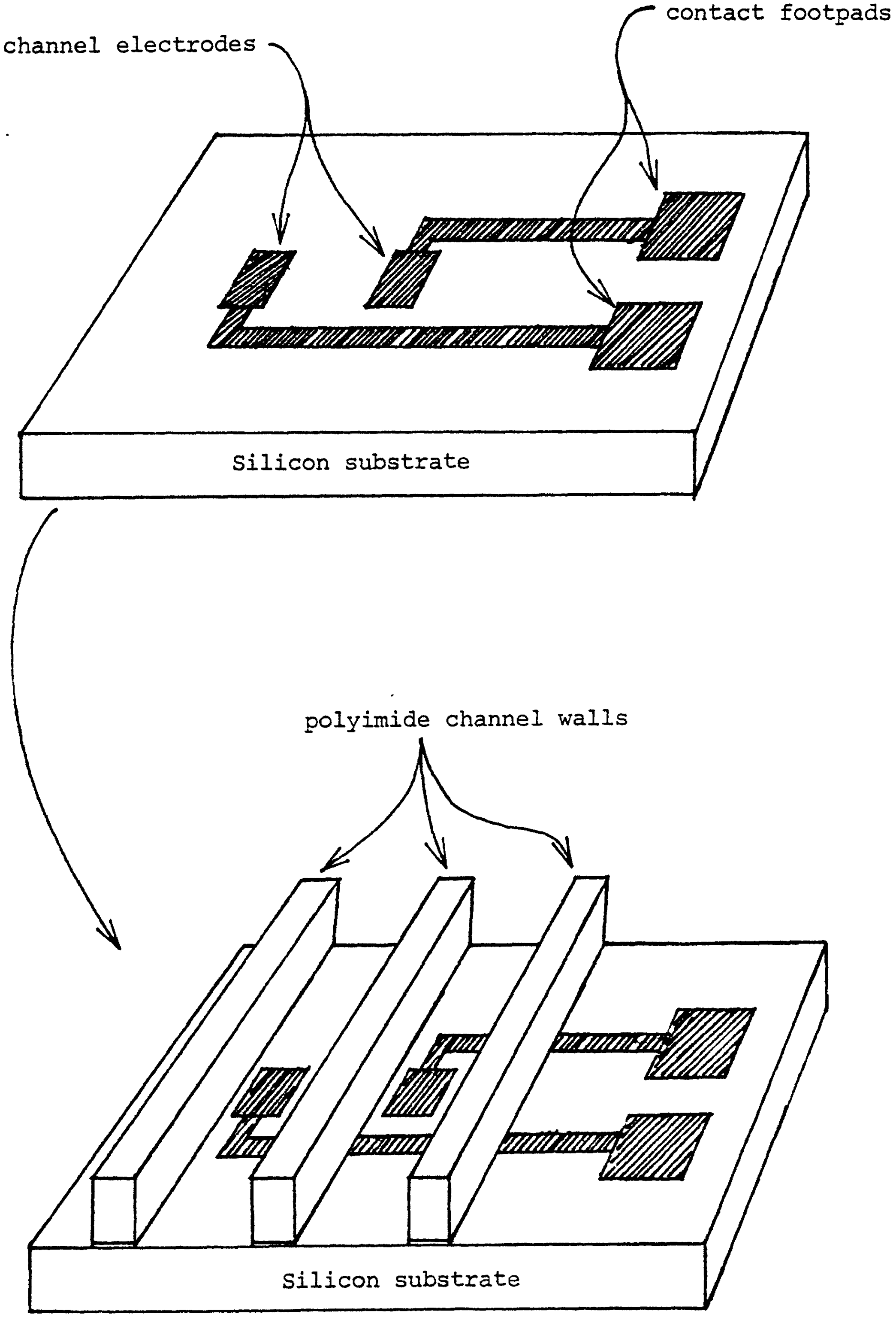

Figure 3-9: Planar electrodes with subsequently etched channel walls.

polyimide equivalent to a photoresist mask on a planar substrate.

The only problem with this method is that it is very time consuming. The etch rate of polyimide under the conditions we used is on the order of 7um/hour. Our moats are considerably deeper than 7um so an etch to substrate might last five or six hours for each mask level. Also, cured polyimide is difficult to strip from a planar silicon dioxide surface, let alone an irregular one. It is for this reason that the single polyimide etch step in the laying of channel walls was chosen over the polyimide mask method.

Maximum mask size consideration in our lab permitted 12 parallel channels 50um wide on 75um centers and 12 150um x 150um footpads for bonding signal output wires. Such large channels were chosen to ease the regeneration process. For this configuration, electrical leads which connect each electrode to one footpad are forced to run through the bottom of other channels in the finished device, therefore these leads have to be passivated everywhere except for the electrode face and the connection footpad.

There are two alternatives in the implementation of such a structure. The first and simplest would be to generate a noble metal electrode pattern on a thermally oxidized wafer surface. Atop this pattern would be placed a low temperature oxide and then a nitride layer. Contact windows could then be etched to the electrode faces and the connection footpads leaving the remainder of the leads insulated as they passed below the channel*. This concept is illustrated in figure 3-10.

Unfortunately, no low temperature oxide system was available in our laboratory at the time of this research so the alternate route had to be followed wherein p^+ diffusion leads are laid in a lightly doped N-type substrate**. A thermal oxide is grown and contact windows opened at both ends of the leads. Noble metal electrodes and footpads are patterned atop the contact windows and the planar part of our device is complete. This implementation is illustrated in figure 3-11.

There are a few disadvantages to this method. The first is seen in the fact that we have created a direct electrical contact between our electrodes and the substrate. In fact, our diffusion lead-substrate contact is a diode with back bias leakage current***, and a parasitic junction capacitance. In addition, since the resistance between footpad and electrode must be kept relatively low, we are forced to use wide diffusion leads which prohibits making very small devices. These characteristics and their effects on device performance must be examined.

---

*At this point, the channels would not actually be on the device.

**p^+ in n rather than n^+ in p was chosen since Na^+ contamination could form an inversion layer shunt between the n^+ regions in the p substrate.

***Due to the level of the signals expected, we will consider operation about zero volts bias; a voltage for which the diode is back biased.

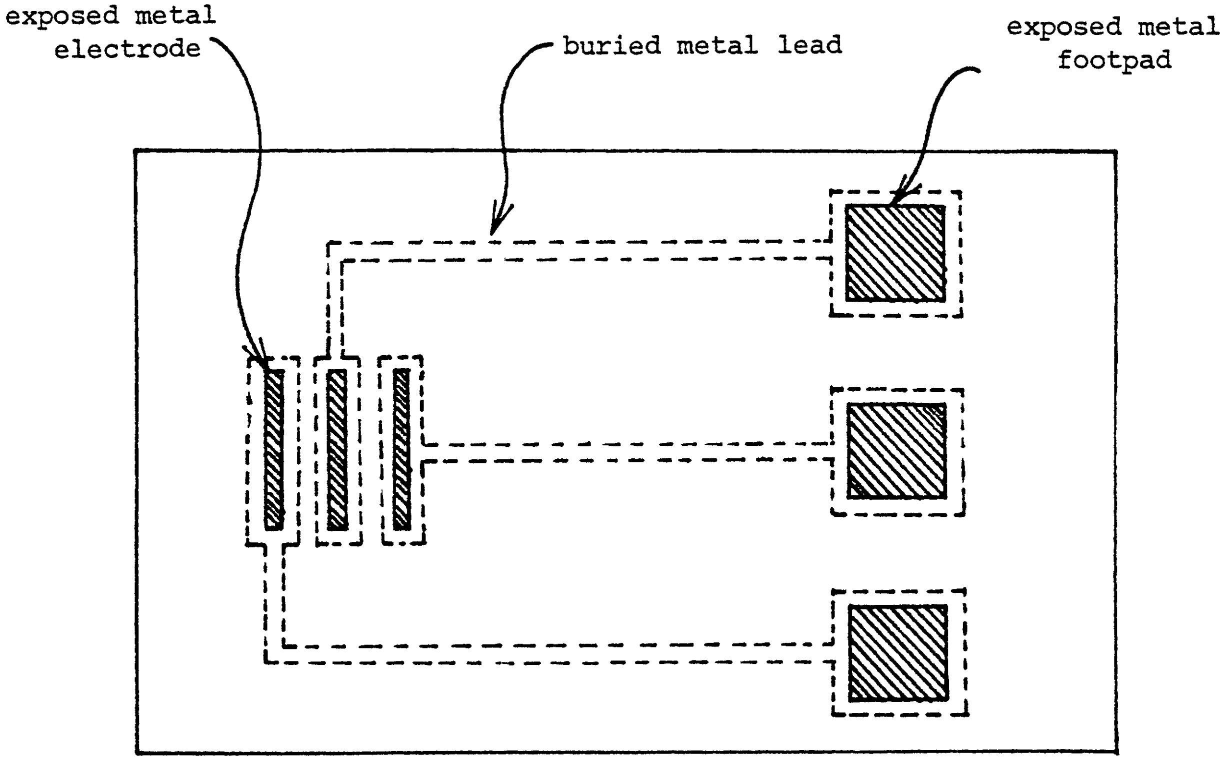

top view

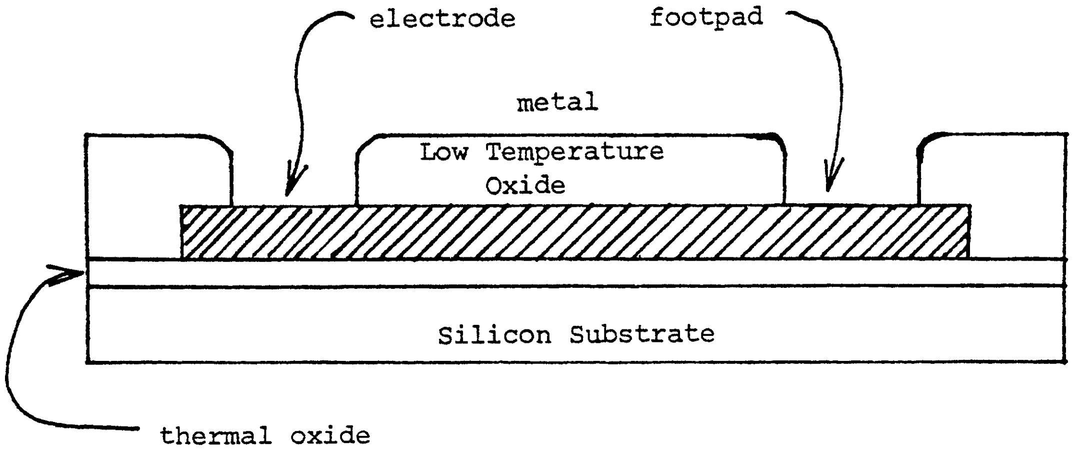

side view

Figure 3-10: Noble metal electrode pattern with contact windows etched in oxide.

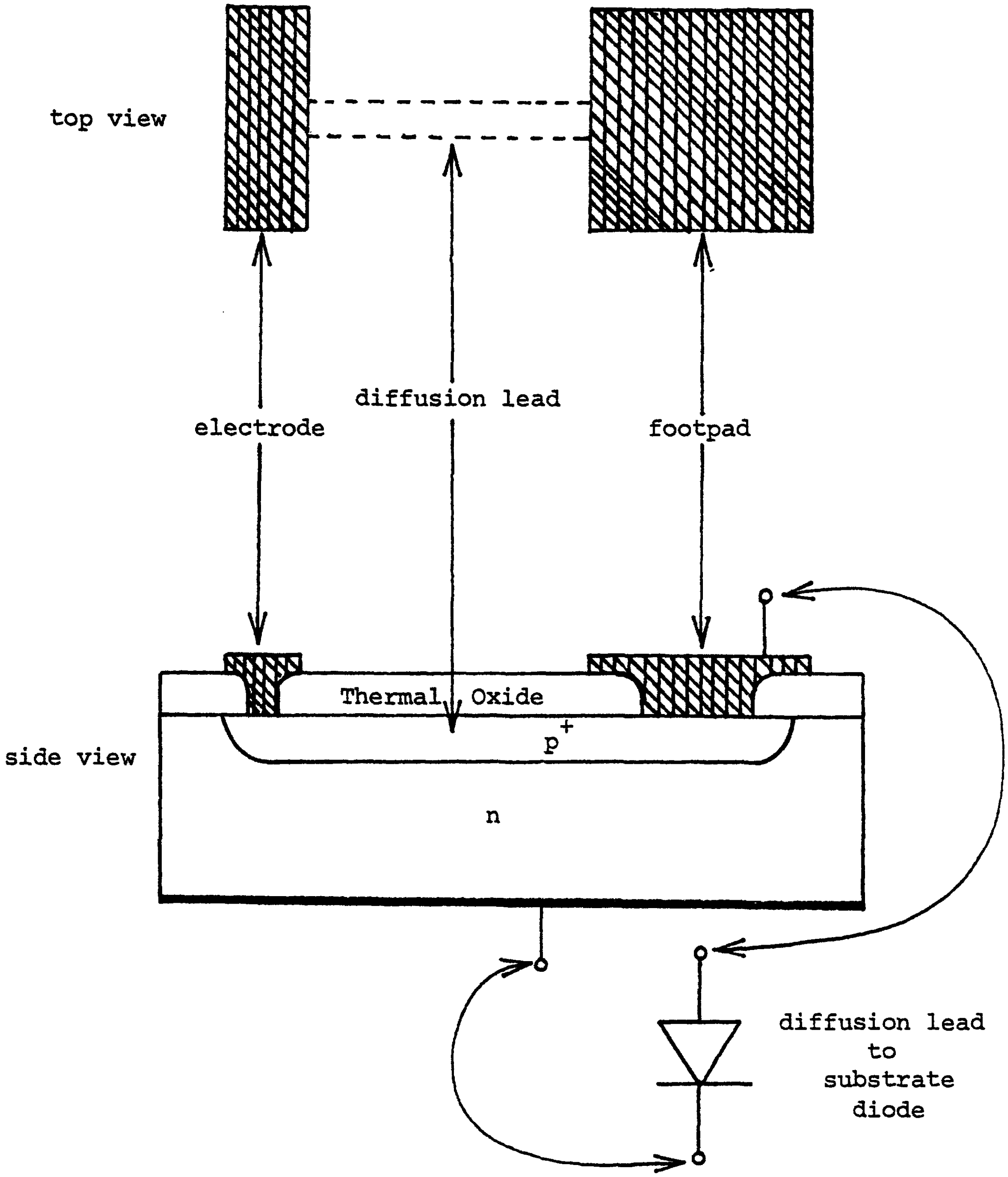

Figure 3-11: Metal footpad and electrode connected via a diffusion lead.

Let us consider the diode first. We would like low back bias leakage current as a function of bias voltage and a low junction capacitance. Are these two design objectives compatible? A junction of lightly n doped and highly p doped silicon forms a thick depletion layer in the n type material. This tends to produce low junction capacitance, however, hole-electron pair generation in the depletion layer contributes to leakage current, and the depletion layer thickness is a function of bias voltage. We must examine the situation more closely. In the following analysis the temperature is considered to be 300^{o}K.

Assume a substrate bulk resistivity of 10ohm-cm. In an n-type material this implies an impurity concentration of about $4\text{x}10^{14}/\text{cm}^3$. Assume a p^+ channel resistivity of 100ohm/square and a channel depth of 5um. This implies a bulk resistivity of $5\text{x}10^{-2}$ ohm-cm and an impurity concentration of approximately $2\text{x}10^{18}/\text{cm}^3$. As a first order approximation let us assume an abrupt junction.

First we need to know the depletion region width. This is given by,

$$3.1 \qquad W_D \simeq \left[\frac{2(\phi_o-\phi)\varepsilon_{si}}{qN_D}\right]^{\frac{1}{2}} \qquad \text{for} \quad N_D \ll N_A$$

where $\phi_o = \frac{-kT}{q}\ln(n_{po}/N_D)$

n_{po} - minority carrier concentration in p material

N_D - donor concentration in n material

ε_{si} - permitivity in Si (1.03×10^{-12} F/cm)

q - electronic charge (1.6×10^{-19} coulombs)

k - Boltzman constant (1.38×10^{-23} joule/$^{\circ}$K)

T - temperature in $^{\circ}$K

ϕ - applied potential across diode contacts (p^+ to n)

The leakage current generated in the depletion layer is*,

$$I_L = (-qAW_D n_i/2\tau_o) \tag{3.2}$$

n_i - intrinsic carrier concentration (1.6×10^{10})

A - junction area

τ_o - excess carrier lifetime

---

*There is also a constant term due to generation in the quasi-neutral regions of the bulk which we will neglect here since we seek the change in the current with applied potential

The charge in the depletion layer is given by

3.3 $$Q = -qAW_DN_D$$

We also know that,

3.4 $$R_L = 1/(\frac{dI_L}{d\phi})$$

and

3.5 $$C_j = \frac{dQ}{d\phi}$$

Thus we obtain,

3.6 $$R_L = (\frac{2\tau_o}{qAn_i})/(\frac{dW_D}{d\phi}) = (\frac{4\tau_o}{qAn_i})(\frac{qN_D}{2\varepsilon_{si}})^{\frac{1}{2}}(\phi_o-\phi)^{\frac{1}{2}}$$

and

3.7 $$C_j = qAN_D(\frac{dW_D}{d\phi}) = (qAN_D/2)(\frac{2\varepsilon_{si}}{qN_D})^{\frac{1}{2}}/(\phi_o-\phi)^{\frac{1}{2}}$$

For ϕ small these equations become,

3.8 $$R_L \simeq (4\tau_o/qn_iA)(qN_D\phi_o/2\varepsilon_{si})^{\frac{1}{2}}$$

3.9 $$C_j \simeq (qA/2)(2\varepsilon_{si}N_D/q\phi_o)^{\frac{1}{2}}$$

Using a typical carrier lifetime of lus* and junction area of $5\mathrm{x}10^{-4}\mathrm{cm}^2$ we obtain $R_L = 1.45\mathrm{x}10^{10}$ ohms and C_j=3.4pF.

We now have an idea of the range of values expected. Let us be slightly more exact. Previously we assumed an abrupt junction. This is almost never the case. Again, assuming a junction depth of 5um we look to the Lawrence-Warner curves for a Gaussian impurity distribution into constant background (Hamilton & Howard 1975 pp132). With impurity concentrations as before this gives directly a depletion layer width of 3um and a junction capacitance of $6.5\mathrm{x}10^3\mathrm{pF/cm}^2$. For our assumed junction area of $5\mathrm{x}10^{-4}\mathrm{cm}^2$ this yields C_j=3.25pF. Thus our initial approximation was reasonable for determining the junction capacitance. For our purposes, 3pF is negligible..

An additional source of leakage occurs due to surface states around the perimeter of our diffusion region (Grove 1967). The current in this region is given by,

$$I_S = -qA_SU_{S/2} \tag{3.10}$$

U_S - net surface generation/recombination rate per unit area
A_S - surface area of depleted region

---

*Gray & Searle (1969 pp66) give a range of 3ns to 500us for the excess carrier lifetime. Colclaser (1980 pp118) gives 1 to 5us as a typical silicon lifetime.

The surface area A_S would be the product of the depletion width W_D and the diffusion region perimeter L. As before we see that,

$$3.11 \qquad R_S = \left(\frac{dI_S}{d\phi}\right)^{-1} = (1/qU_S L)(qN_D/2\varepsilon_{si})^{\frac{1}{2}}(\phi_o - \phi)^{\frac{1}{2}}$$

Assuming a surface totally depleted of majority carriers, the value of U_S for our n-type region with doping $4\text{x}10^{14}/\text{cm}^3$ is $U_S=8\text{x}10^{10}/\text{cm}^2$*. If the perimeter L=2mm then about a bias of $\phi=0$, $R = 2\text{x}10^{12}$ ohms. This is substantially larger than the previously calculated R_L. Since R_S and R_L are effectively in parallel, R_L will dominate the back bias resistance, so we can expect this value to be on the order of $1.5\text{x}10^{10}$ohms. This is acceptable for our purposes.

The next design parameter we must consider is that of electrode area. Since coupling to the saline solution is mostly capacitive for a noble metal electrode (Dymond 1976), (Robinson 1978), the area should be as large as possible so as to lower the impedence, but we do not wish to interfere with the electric field in the channel so we cannot make the electrode too large. Let us try an electrode which is 10% of the channel length and exactly as wide as the channel. (The electrode of Mannard & Stein 1974 seems to have been fashioned thus). For a 1mm long 50um wide channel this gives an area of 5000 um^2. Robinson (1968) and Dymond (1976) concur that capacitance values for inert metal electrodes in a

---

*Derived from Grove 1967 pp136-148. n_s, p_s and $p_n(0)$ are taken to be zero due to depletion.

physiological saline solution (.9%NaCl by weight) range from $.1pF/um^2$ to $.2pF/um^2$ at 1 KHz for untreated surfaces. If the surface is treated to make it more irregular, thereby increasing the surface area, these values may increase by as much as 300 times to $60pF/um^2$ (Robinson 1968).

Using the worst case of $.1pF/um^2$ we see that our electrode has a capacitance of 500pF. For operation at 200Hz using an amplifier with 10 Mohm impedance, a saline/electrode coupling capacitance of greater than 80pF would be sufficient.* A theoretical electrode capacitance of 500pF would serve admirably.

The only design consideration left is that of which noble metal to use. Gold is very inert (Edell 1980) and since it was the only noble metal available, gold was chosen. Gold does not adhere well to silicon dioxide, so a two layer metalization must be used. Aluminum, molybdenum and chromium were available. Aluminum/gold did not adhere well and molybdenum/gold will corrode in saline (Edell 1980) Maussel & Glang 1970).

Chromium has excellent adhesion properties and forms ohmic contacts with silicon (Harper 1970). Chromium also forms a very tough oxide layer immediately upon exposure to atmospheric oxygen and this layer is very inert in a physiological environment (Loeb et al 1977). However, if current passage through exposed chromium oxide proves to be a problem (Loeb et al 1977) the first processing technique mentioned of metal electrodes buried under an oxide-nitride film could be

---

*The cutoff point was chosen to be that value of the electrode capacitance for which the impedance at 200Hz equaled the input impedance of the amplifier used to totally isolate the chromium undercoat. In short, chromium contamination was not deemed such a toxicity threat as to preclude its use in our devices: at least not in amphibia.

Figure 3-12 shows the first two steps in the fabrication of our planar array of 12 electrodes. Figure 3-13 shows a complete planar electrode array on a silicon substrate. The small rectangles on the metalization pattern are the channel electrodes. In figure 3-14 we see the aluminum mask on a polyimide layer which is used to etch the channels and in figure 3-15 we see a finished device with polyimide channels, central gold electrodes and external connection footpad. Complete process specifications were considered too lengthy for inclusion here and can be found in the appendix.

The device is now almost complete. We must cover the moats to create channels, attach a connection cable and equip our electrode with a nerve-guide cuff for implantation. Moat coverage was accomplished by spin coating a thin film (2 to 3um) of polyimide onto the 150um thick glass cover slip. The device was then laid onto the cover slip. The result is hown in figure 3-16.

Next we attach a connection cable. We would like the cable cross-section to be as small as possible. Since individual wires must be isolated from one another, one method would be to bond small insulated wires directly to the device (Edell 1980). Unfortunately, insulated wires of the proper

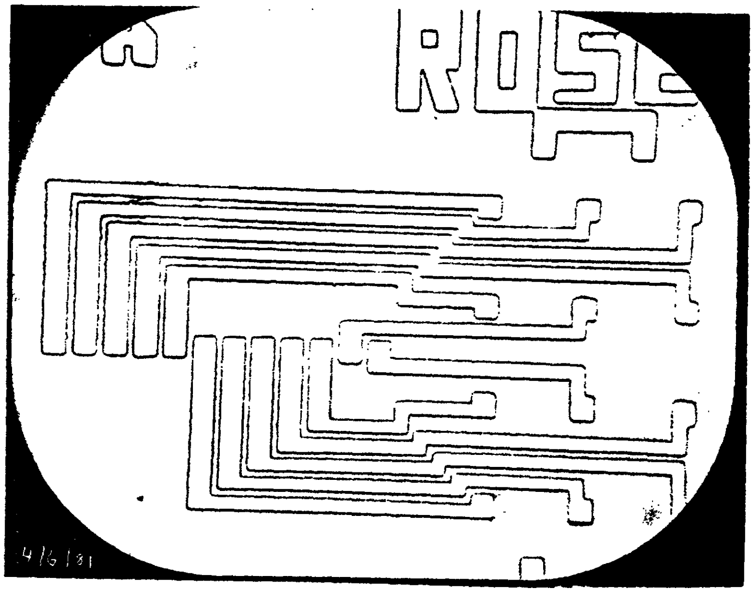

a) diffusion lead mask in oxide.

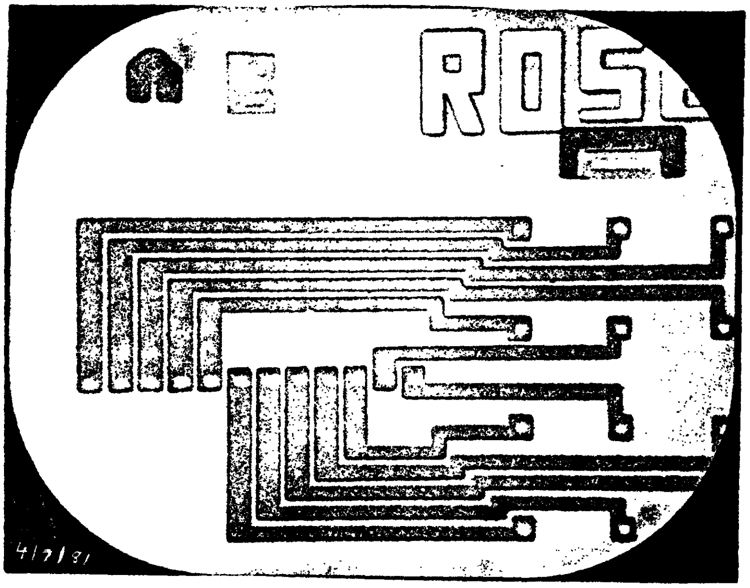

b) diffusion leads with contact windows.

Figure 3-12: Mask levels A and B.

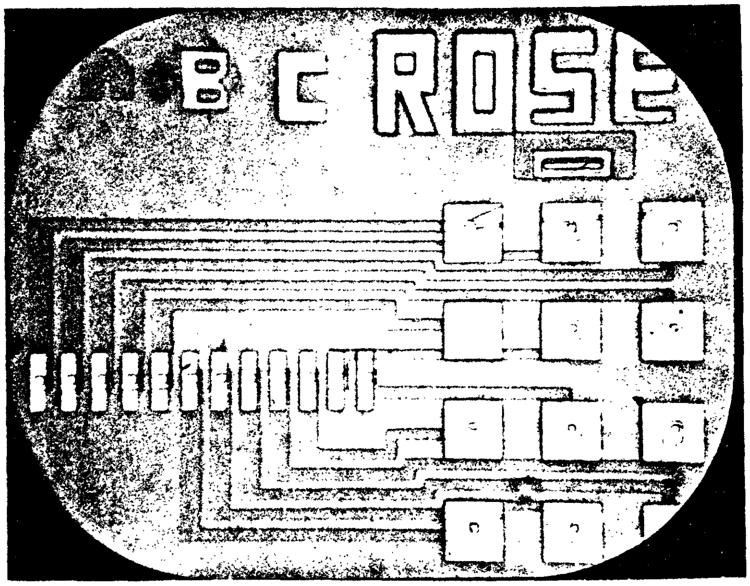

Figure 3-13: Metalized planar electrode. Footpads are 150um square. Electrodes are 150umX50um.

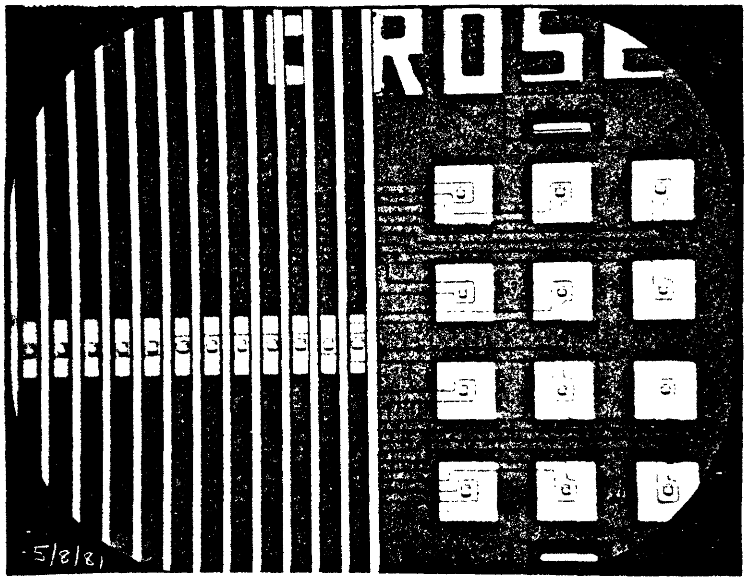

Figure 3-14: Aluminum moat mask atop polyimide, aligned to underlying electrode pattern.

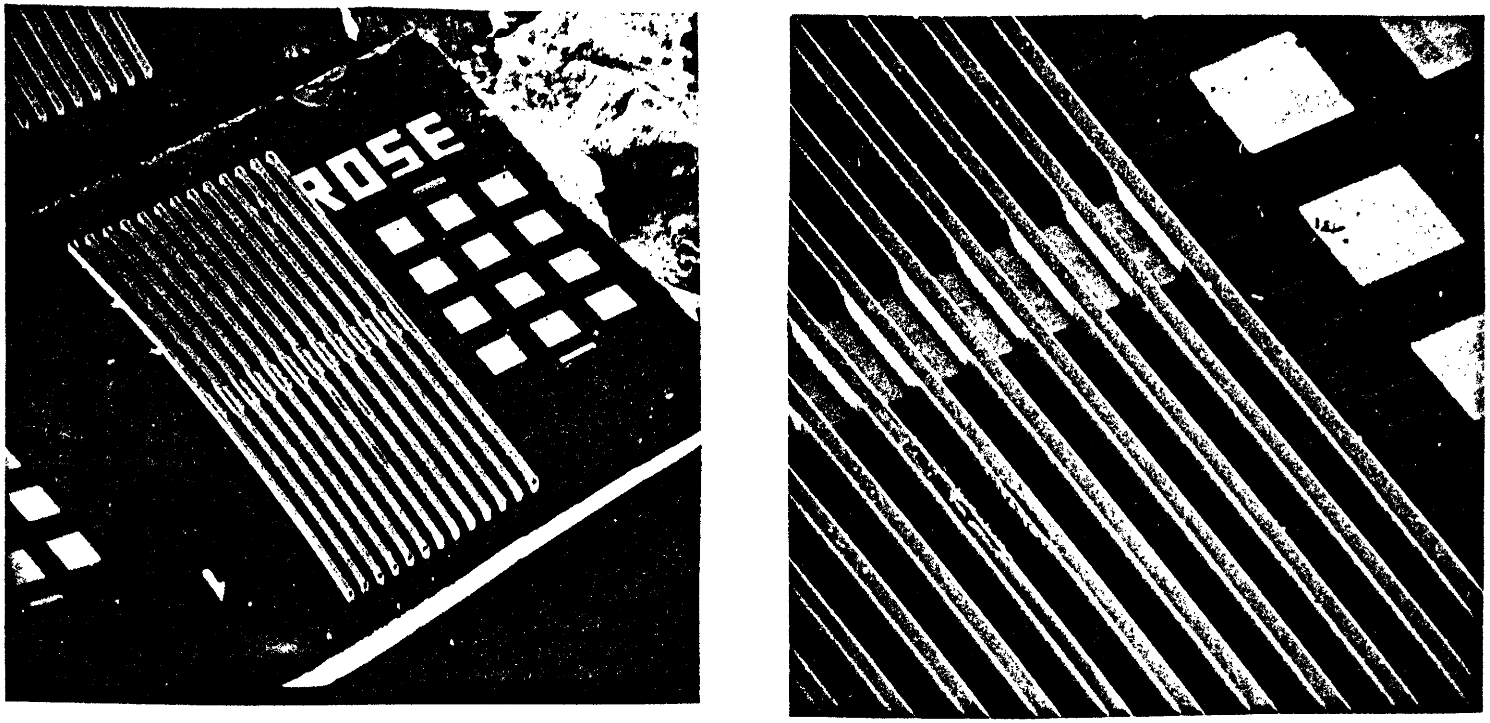

Figure 3-15: Planar electrode with polyimide ridges. Ridges are 50um high and 25um wide.

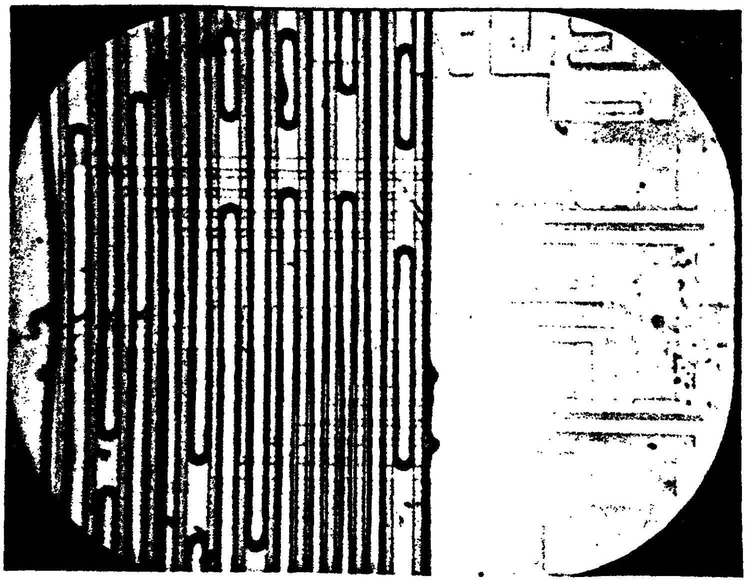

Figure 3-16: Glass coverslip attached to moats with a thin film of polyimide. Some beading is evident but it does not occlude the channels.

dimensions and metal (silver, aluminum, gold) were either very expensive or unavailable so we opted to make our own wire cables.

Rudimentary test cables consisted of five 25um diameter gold (or aluminum) bonding wires embedded in a thin layer of Bostik 4025 Nitrile-Rubber adhesive. Once dry and thermoset, this adhesive is reasonably inert. One end of the cable was bonded to a header, the other to the device using an ultrasonic wedge bonder. Three such cables were used per device with one wire from each cable contacting the substrate. The contact pads were then coated with more Bostik 4025 to both fasten them to the substrate and insulate them from the saline solution in which the device was to be tested.

Another more implantable version would consist of coating the bonding wires with a thin layer of soft epoxy. The insulated wires thus obtained would be bonded as before using the ultrasonic bonder. The complete cable would be then recoated with soft epoxy. In figure 3-17 is shown our concept of a device with an attached cable. A superior version of this device would use medical grade Silastic (Dow Corning) encapsulation. Silastic is a very tractable material frequently used in implants (Boretos 1973).

Finally, a cuff may be fashioned using a thin sheet of Silastic mounted initially with Eastman 910 a biodegradable (Boretos 1973) adhesive. A more secure permanent mount could be

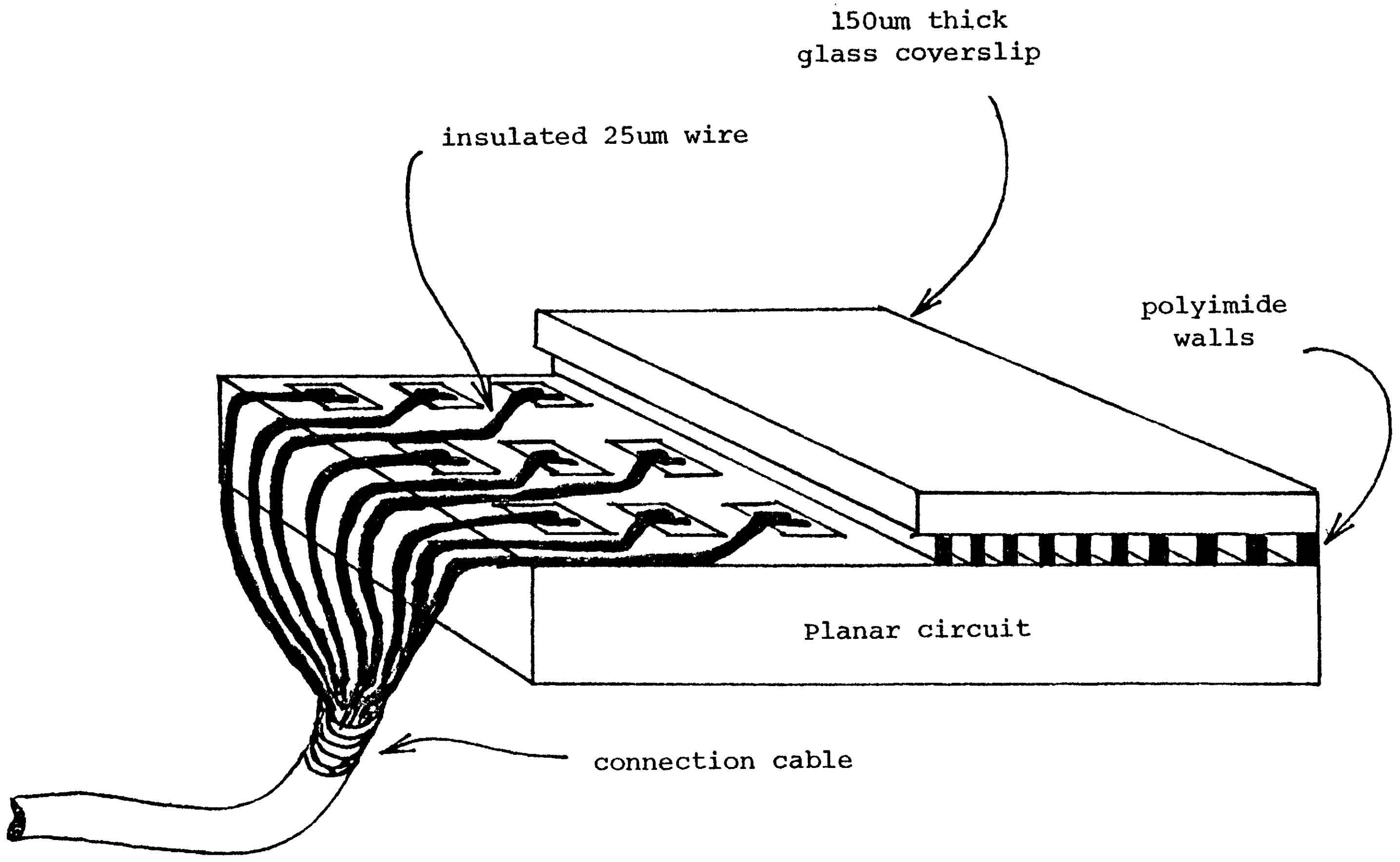

Figure 3-17: Regeneration electrode with soft epoxy cable.

made with polyimide. The complete regeneration electrode is shown in figure 3-18.

We turn now to Chapter 4 where we characterize the device.

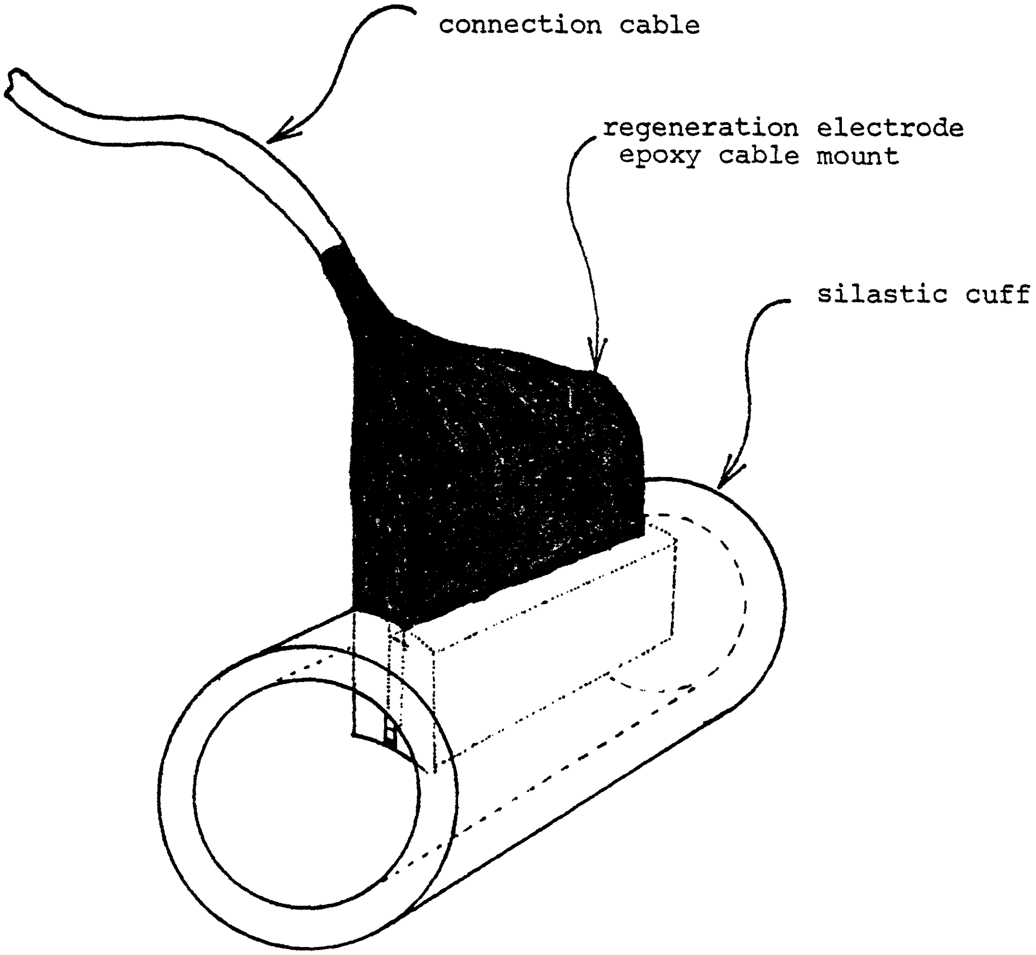

Figure 3-18: Cabled regeneration electrode with nerve guide cuff.

CHAPTER 4

In this chapter, the physical and electrical characteristics of our device are presented. Figure 4-1 shows the planar device with the twelve electrodes and footpads identified by number. Figure 4-2 shows a cross-section of one electrode immersed in a saline solution and gives the associated distributed circuit model.

The physical parameters of interest are (1) the number of squares per diffusion lead 2) the junction area 3) the sheet resistance of the diffusion layer 4) the junction depth 5) the diffusion doping 6) the substrate doping and 7) the oxide thickness. These are listed below.

Lead No.	squares/lead	junction area
1	50	$4.80x10^{-4}cm^2$
2	60	$5.25x10^{-4}$cm2
3	68	$5.56x10^{-4}$cm2
4	62	$5.00x10^{-4}$cm2
5	36	$3.18x10^{-4}$cm2
6	34	$3.20x10^{-4}$cm2
7	44	$4.25x10^{-4}$cm2
8	52	$4.50x10^{-4}$cm2
9	48	$4.12x10^{-4}$cm2
10	20	$2.20x10^{-4}$cm2
11	26	$2.00x10^{-4}$cm2
12	24	$1.50x10^{-4}$cm2

diffusion layer sheet resistance = 100 ohm/square
junction depth - 3um, diffusion doping - $5x10^{18}/cm^3$
substrate doping - $4x10^{14}/cm^3$,
oxide thickness- 5000Å (1000Å over diffusion)

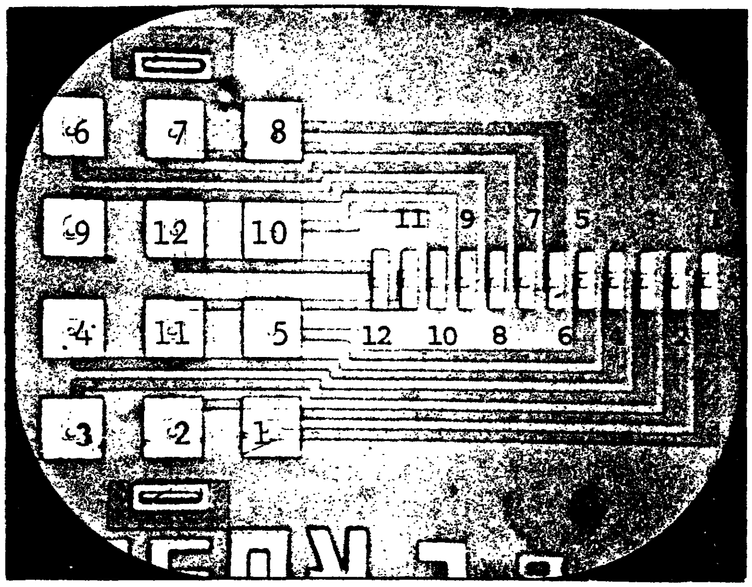

Figure 4-1: Planar device with lead identification numbers.

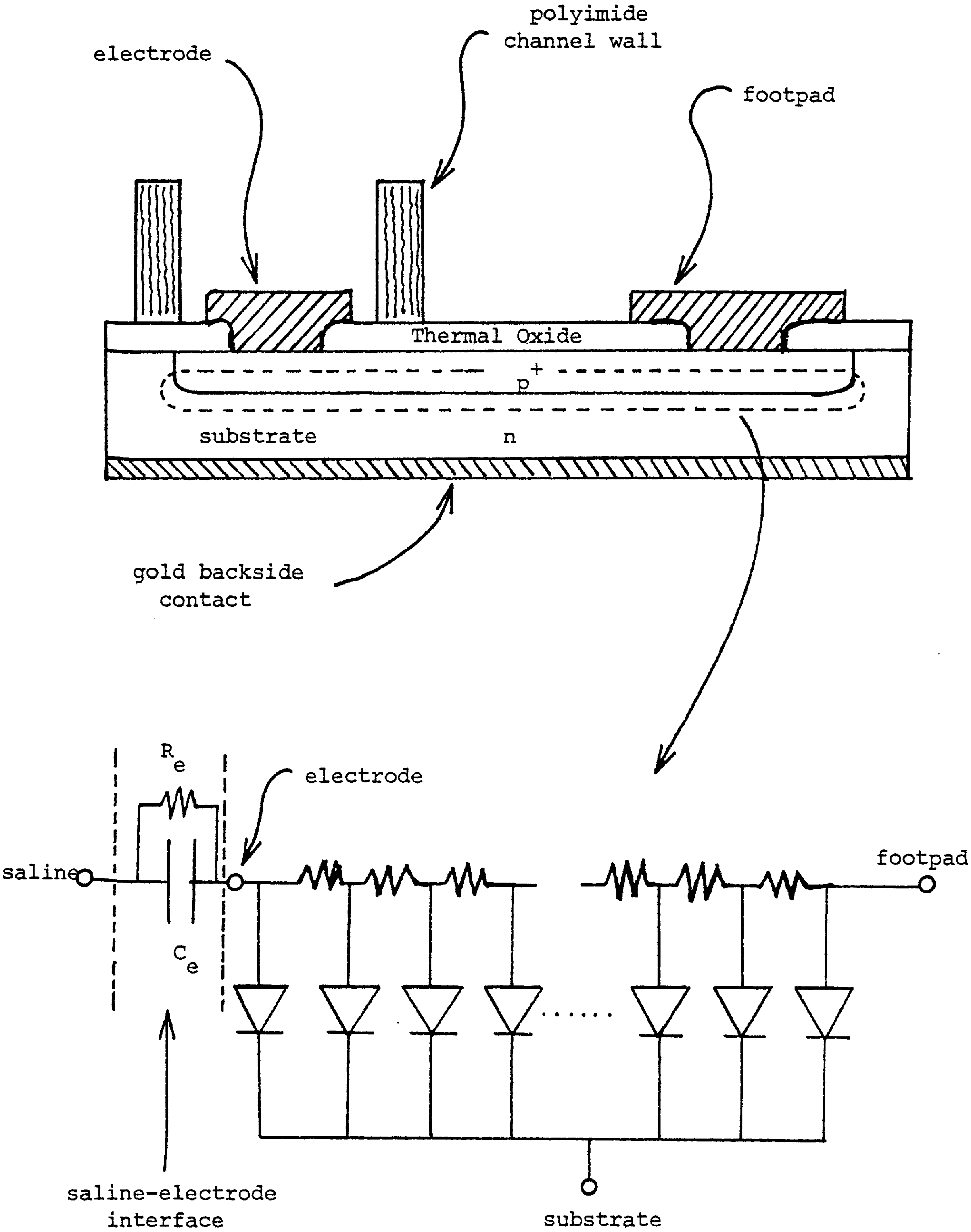

Figure 4-2: Cross-section of electrode immersed in saline and the equivalent circuit model.

The electrical parameters of interest are the V-I characteristics of 1) diffusion resistance 2) diffusion to substrate resistance and 3) interelectrode resistance. Also of interest is the junction capacitance, the electrode-saline capacitance as well as the intrinsic noise level of the device in air and physiological saline for the planar device before the reactive ion etch step where the channel walls are formed.

Figure 4-3a, b and c show the diffusion resistance, junction diode, and interelectrode current-voltage characteristics respectively for the planar device prior to 0_2 plasma etching.* In addition, the diffusion lead resistance, the junction capacitance, and the saline-electrode capacitance** are listed below.

Lead No.	Lead Resistance	Junction Cap. 1MHz / 1KHz		Saline-elect. Cap. (1KHz)
1	5.00Kohm	6.0pF	--	222pF
2	5.72Kohm	6.4pF		222pF
3	6.17Kohm	6.8pF	6.5pF	206pF
4	6.25Kohm	6.2pF	--	222pF
5	3.91Kohm	4.4pF	--	254pF
6	3.69Kohm	5.0pF	--	222pF
7	4.65Kohm	5.4pF	--	238pF
8	5.08Kohm	5.8pF	6.0pF	--
9	4.60Kohm	5.4pF	--	254pF
10	2.93Kohm	3.3pF	--	222pF
11	3.11Kohm	3.4pF	--	254pF
12	2.63Kohm	3.2pF	--	270pF

---

*All V-I characteristics are measured in darkness to avoid surface generation.

**Measurement system described in appendix

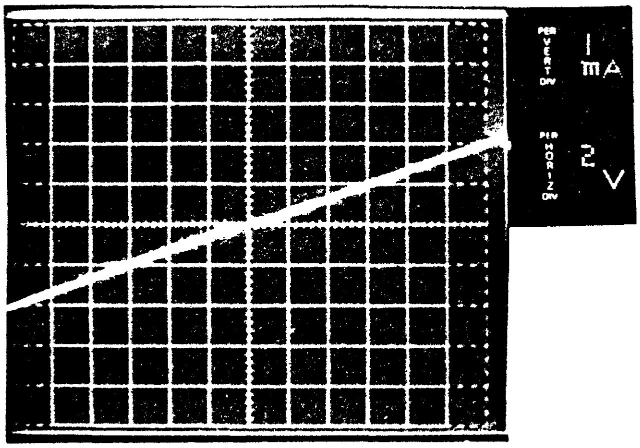

a) footpad to electrode V-I characteristic (substrate floating).

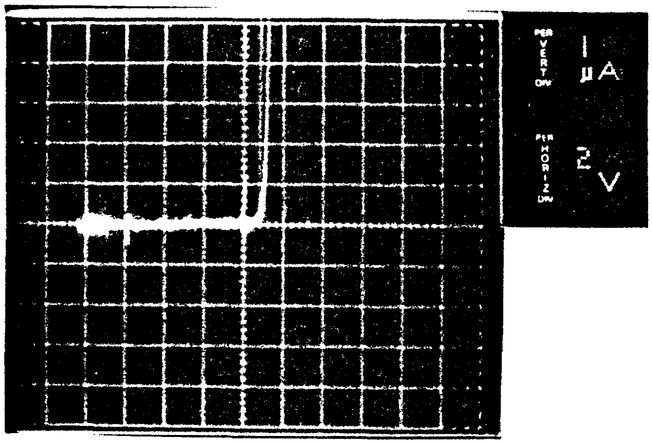

b) footpad (or electrode) to substrate V-I characteristic.

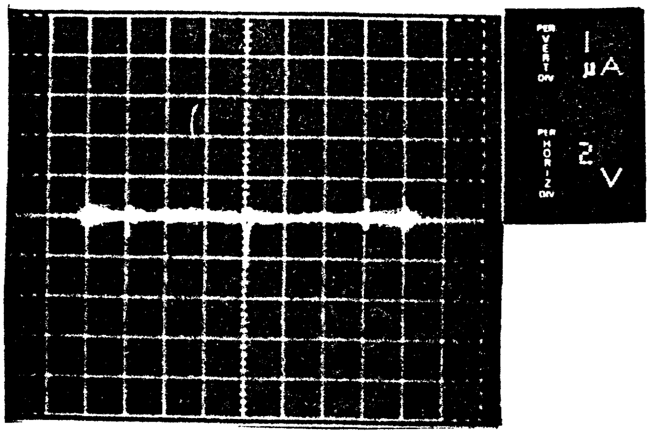

c) Inter-electrode (or footpad) V-I characteristic (substrate floating).

Figure 4-3: p^+ on n with thin oxide device characteristics.

The back bias resistance of the diode as well as the interchannel resistance was approximately 100Mohm with circuit surface illuminated much greater than 100Mohm in darkness as measured with an ohmmeter. All of these measurements except the electrode-saline capacitance are in agreement with the expected values given the physical characteristics of the device.

The dimensions of the gold electrode are 50um x 150um x 1.5um. With one 50um x 150um face exposed this gives a surface area of 8100um^2 . Using the worst case capacitance value of.1pF/um^2 from Chapter 3 we should have at least 810pF in physiological saline. As seen in the table, we obtained on the order of 240pF. This implies a capacitance per unit area of approximately .03pF/um^2. As a check, the electrode surface was recleaned in acetone and methanol to remove any oils or other organic contaminants which could act as insulators thereby decreasing the effective area. The result was the same.

One explanation for this discrepancy may be semantic. Robinson (1968) describes the tested surface as "bright" platinum. No mention is made of exactly how irregular the surface is. If the "bright" platinum electrodes are machined or otherwise worked mechanically, chances are that the electrode surface is not as smooth as our metal surface which is evaporated onto a highly polished device-grade silicon wafer*. That being the case, a "bright" platinum surface has effectively more surface area than our electrode surface. This would be evidenced by an increase in the measured capacitance per unit area relative to our devices.

This difference, though sizeable, should not interfere with our recordings. In addition, after the 0_2 plasma etch step, the gold surface will be roughened and the capacitance per unit area should rise if the original highly polished gold surface is the problem.

Root mean square thermal noise voltage for a 10KHz bandwidth at 300^{o}K was measured for our device in air and in saline solution**. The measurement system was calibrated on 5Mohm, 500 Kohm and 50Kohm precision resistors, and both open and short circuits. The short circuit generated the minimum observable noise level for our system of .13uV. This noise was generated by the bandpass filter at the output of the amplifier (please appendix for details). An open circuit produced the same minimum reading. This is not surprising since the amplifier requires some non-zero input bias current and an open circuit cannot supply this current. This argument applies to very large resistors as well.

---

*According to Hamilton & Howard (1975), the wafer surface is first ground optically smooth and then through a series of mechanical-chemical polishing steps, almost all surface defects are removed.

**Measurement system described in the appendix

According to Gesteland et al (1959), the thermal noise generated by a metal electrode is equal to the thermal noise generated by a resistor whose value is the real part of the electrode impedance. The p^+-n junction resistance is effectively an open circuit (greater than 100Mohm) so we may neglect it. The electrode resistance for a bright noble metal is, as given by Robinson (1968), $1.33\text{x}10^6$Mohm/um^2,thus our electrode, whose exposed surface area is about 8000um^2, has a resistance of 166Mohm. In view of our unexpectedly low electrode capacitance, this resistance may be as high as 560Mohm. This too is effectively an open circuit to any amplifier we may use.

Therefore, as expected, the device in both air and saline produced the open circuit reading of .13uV. The noise generated by our device cannot drive our amplifying circuitry, whereas the signals we wish to record can, so thermal noise generation by the device should cause no problem.

After the planar devices underwent 0_2 plasma etching down to the planar substrate, they were retested. A marked degradation of device performance was seen. Figure 4-4 shows a junction after the reactive ion etch. Notice in particular the poor back bias characteristic. This is intolerable in a device where channel-substrate isolation is necessary in order to foster interchannel isolation.

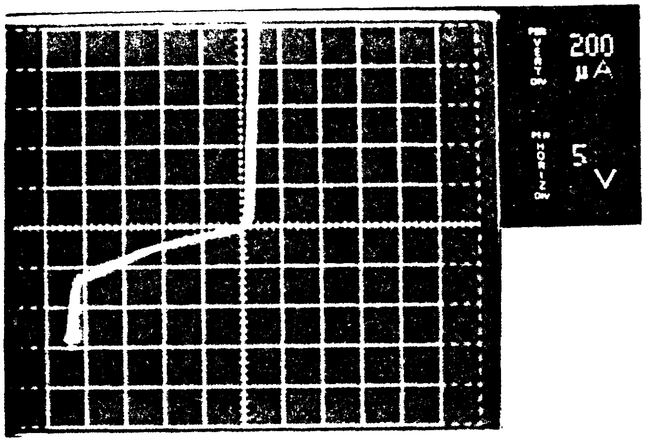

Figure 4-4: Footpad to substrate V-I characteristic after O_2 plasma etch of polyimide channel walls. (p^+ on n thin oxide)

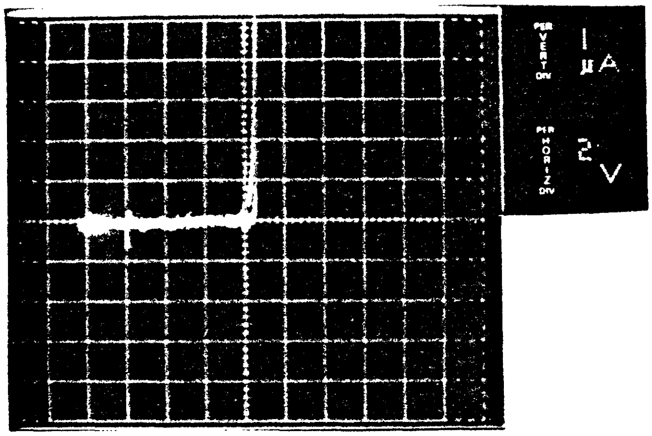

a) before etch

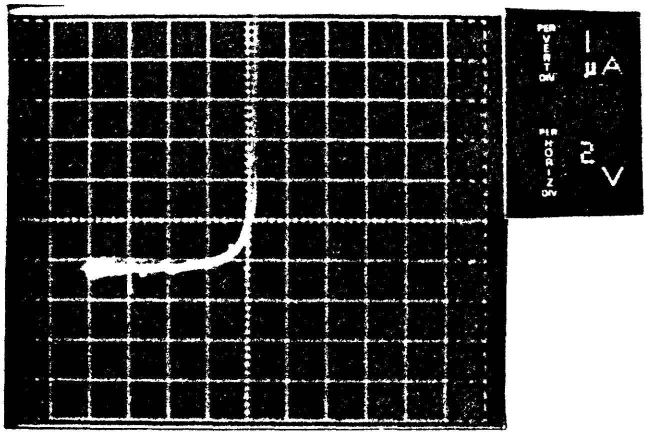

b) after etch

Figure 4-5: n^+ on p device with 5000Å oxide. Footpad to substrate V-I characteristic.

If the etch was stopped just short of completion* so that a thin coating of polyimide (approximately 1um) remained over the electrodes, the device was left unaffected**. It was only if the polyimide was completely etched that degradation was seen. Due to the uneveness of the polyimide coating, the time for "etched to completion" varied over the wafer surface. It was primarily in those parts which had etched more quickly, and were therefore exposed to 0_2 plasma for a longer period of time, that the greatest amount of back bias leakage was seen.

This fact implied that some sort of surface damage was occurring due to direct exposure to the 0_2 plasma or the U.V. radiation produced by it. To test this hypothesis, device wafers with no polyimide coating were placed in the plasma etcher under the same conditions as for the polyimide etch for one hour and twenty minutes. This was the maximum exposure time of the devices which etched "quickly" as described in the preceding paragraph. Surprisingly, the devices remained perfectly intact. There was no difference in their characteristics before and after exposure to the plasma. Thus it would seem that some by-product of the 0_2-polyimide reaction was necessary to cause junction breakdown. This hypothesis has not been tested.

---

*This is due to the uneveness of the applied 50um polyimide layer rather than to etch depth control on our part.

**The electrodes were reached by punching a hole through the thin polyimide layer with a needle probe.

It was at this time that previously made n^+ channel on p substrate devices were examined. These devices had been fabricated and then tested using only an ohmmeter to measure lead resistance and the like. Like the p^+ on n devices, a resistive shunt between channels was observed, however, through an oversight, no explicit V-I curves were obtained at that time. Other than the obvious difference in substrate types, the n^+ on p and the p^+ on n devices differed in only two respects. For the n^+ on p devices, the oxide over the diffusion region was 5000Å thick and the plasma etch of the polyimide was carried out at 80 watts versus a 1000Å thick oxide over the diffusion region and an etch at 150 watts for the p^+ on n devices.

Figure 4-5a and b show a junction characteristic for the n^+ on p device both before and after the etch. Notice that the after-etch curve does not display the severe junction degradation of figure 4-4. Notice also the more rounded "soft knee" and the back bias leakage current of 1uA which remains constant with back bias voltage. These two observations seem to imply excess surface states probably due to radiation damage of the silicon surface. The damage in this case, however, is not as pronounced as with the p^+ on n devices with thin oxide and high etch power. It is felt, therefore, that the problem of severe junction degradation illustrated in figure 4-4 may be combated by using thicker protective oxides over the diffusion region (1um) and a lower etching power during our reactive ion etch.

Thick oxide p^+ on n devices were fabricated but due to equipment malfunctions, polyimide ridges were not etched on these devices. It remains to be seen whether this scheme will prove successful.

With relatively thick protective oxides (5000Å) we may still have some V-I characteristic degradation as seen in figure 4-5b. Even in a mild case such as this, the interchannel effects are enormous. Figure 4-6 shows the V-I curve for the resistance between two adjacent n^+ diffusions for the device of figure 4-5b (substrate floating). By taking the slope of the curve about zero we see an interchannel resistance of less than 100Kohms. The voltages we expect to record in nerve bundles are effectively in the zero volts bias range and a 100Kohm shunt between channels in unacceptable.

One option, if this effect is indeed due to excess surface states induced by silicon surface lattice damage, is to anneal our devices in a nitrogen atmosphere. We must remember, however, that we have both gold and polyimide on our devices. Polyimide may withstand temperatures of 400°C, but the silicon/gold eutectic temperature is 370°C, therefore we are limited to a low temperature (say 300°C) anneal. This may not prove very useful in removing lattice defects.

Another option open to us is to bias the substrate so that the diffusion lead/substrate diodes are operating in the flat part of the back bias region (less than - 4 volts).

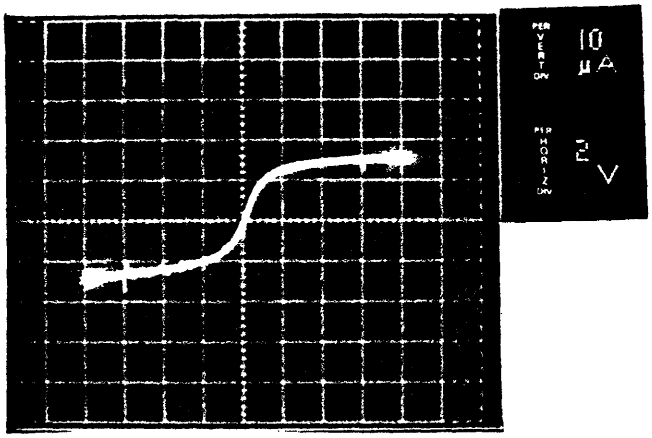

Figure 4-6: n^+ on p device with 5000Å oxide; interelectrode V-I characteristic (substrate floating).

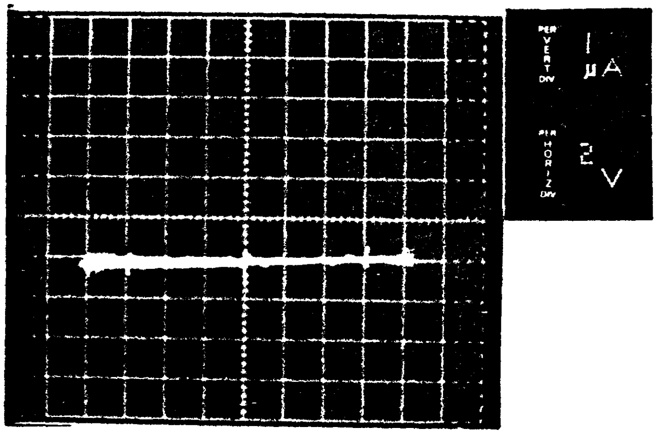

Figure 4-7: Same measurement as figure 4-6 with substrate biased at -15 volts.

This will increase the interchannel resistance. This is illustrated in figure 4-7 where the resistance between the same two adjacent n^+ leads as in figure 4-6 is measured with the substrate biased to -15 volts. Though there is still a leakage of 1uA, the change in current with voltage is effectively nil. This implies high resistance, a fact which is borne out by a resistance of 2Mohm as measured with an ohmmeter for a substrate bias of -5 volts. This is an increase of more than a factor of 20 from the previous value of under 100Kohm.

A third option would be to protect the devices with an aluminum mask over portions which might be exposed to the O_2 plasma. Ephrath and DiMaria (1981) found that a 4000Å coat of aluminum served to protect against damage to the silicon dioxide layer during the reactive ion etching. There is no reason to believe that such a scheme would not also serve to protect underlying circuitry. This method would be particularly useful in the future where high performance circuits will be needed and any type of device degradation after etching would be devastating.

In conclusion, though there are some problems associated with the reactive ion etching step in the fabrication of our regeneration electrodes, and we have therefore been unable to conduct complete electrical testing of a finished device, these problems do seem surmountable.

It is for this reason that we are optimistic about such future applications as densely packed electrode structures utilizing amplifying and multiplexing circuitry on-board.

CHAPTER 5

We have demonstrated that the construction of small channels with central metal electrodes on a silicon substrate is feasible and that the device performs to specifications in a physiological saline bath. The fabrication procedure utilizes standard planar integrated circuit technology and anisotropic etching of polyimide in an oxygen plasma.

The next step is the characterization of the device in living nervous tissue. Here we may take several different approaches. The first and most difficult of these is implantation in amphibian peripheral nerve. Another option as suggested by Peake (1981) is to surgically separate individual fibers from a living nerve bundle and lay them in the channels of our device before afixing the moat lid. This avoids the difficulty of regeneration through the channels and could possibly be used in vivo as well as in vitro. However, it introduces the problem of manipulating delicate individual fibers. The third option is, as mentioned in the abstract, placement of the device sans moat cover in tissue culture. This circumvents both regeneration and tissue handling problems but does not give us isolated channels.

The second and third approaches will probably be used first. Ultimately, the device will be implanted in a regenerating nerve bundle. This could entail the use of a percutaneous button (Edell 1980, Park & von Recum 1981) although a simple transcutaneous cable will probably be sufficient in amphibia.

Let us now explore other possible measurement techniques. Thus far we have considered only voltage measurement. It has been shown that relatively large magnetic fields accompany the propagation of action potentials in peripheral nerve (Gengerelli et al 1961) and a mathematical model of action potential propagation incorporating an inductive element has been presented by Leiberstein and Mahrous (1970). It seems that not much attention has been given to inductive effects in nerve impulse propagation and in some cases such effects are dismissed out of hand. However, techniques designed to record these magnetic fields from individual axons should be developed if only to ascertain the validity of an inductive axon cable model. The concept of the channeled probe seems to lend itself to such an application as it does to voltage measurements.

The success of the electrode presented in this thesis is contingent upon regeneration of nerve fibers through small channels. Channels by their very nature are restricting, and in mammalian preparations, scar tissue can prevent regeneration through the device. We might do well to avoid the use of channels all together if we wish to construct a more "natual" neuroelectric interface.

If axons could be induced to abut an electrode or at least come very near (under 10um) we could dispense with a channel since as shown by Edell (1980), large recorded voltages are theoretically possible in such a recording situation. Such a feat would require axons to exhibit tropism toward the electrodes. Nerve Growth Factor (NGF) in small concentrations causes such tropism. (Levi-Montalcini & Angeletti 1968). This drug, albeit expensive, is commercially available. The next problem is one of delivery: how do we administer NGF to cause the desired effect?

Recently, a technology for continuously delivering controlled quantities of a soluble substance has been developed (Lnager 1981). Langer, in his review article describes four different drug delivery systems: diffusion, chemical, swelling and magnetically controlled processes. Each involves embedding the drug in a suitable biocompatible polymer for release by one of the four mechanisms after implantation. If NGF could be so embedded without altering its properties, small patches of polymer containing NGF could be placed on or near an electrode. This could cause a regenerating nerve fiber to seek the electrode; the desired effect. How to mechanically keep the axon in place once it reaches the electrode is another research problem. One method might surround the electrode with a material to which the nerve or its surrounding tissues will bond.

Now for the ultimate in axonal comfort we have the deluxe synapse board. Soothing tendrils envelop the nerves after a long hard axotomy and usher them to their very own synapse where they may recline at leisure until they regain strength. Thin towers (< 1um square and 10um high) of polyimide could serve as the guide tendrils laid on a suitable silicon synapse circuit grid. Such tendrils may be produced with current techniques (Hawryluk 1981).

A fully compatible neural interface would allow nerve fibers to actually synapse on the active areas of the device. Rather than direct electrical connection, chemical synapses would be used to both record and stimulate. One possible implementation could employ CHEMFETs; field effect transistors equipped with a chemically specific gate (30th ACEMB 1977). A CHEMFET with a gate specifically sensitive to synaptic neurotransmitters could be used to record efferent activity while a controlled transmitter dispersion system would stimulate afferent synapses. At present, such advanced CHEMFETs do not exist (we are limited, at present, to the measurement of a few different ions), but development of a neurotransmitter specific substance for use in the gate of a CHEMFET should be possible eventually.

An even more difficult technological problem is developing the ability to make nerve fibers synapse on something other than living end organs. There seems to be no literature on this topic at present so a "from the ground up" type of methodology in the research of this topic would probably be necessary. A study using 2-D gel electrophoresis (Gall et al 1980) might reveal what substances cause the formation and maintenance of a synapse.

Conceptually, the only drawback with such a recording scheme is the fact that peripheral nerves would not be allowed to reach their original terminations unless a collateral branch was sprouted. This would render the study of information transfer between the CNS and the sensory/motor system in a freely moving animal impossible. Nonetheless, the idea is very attractive for prosthetic applications.

So, in summary, we have shown the feasibility of constructing a small multichannel electrode for implantation in amphibia. In addition we have briefly presented two very interesting alternate structures for a neural interface. These will hopefully warrant further investigation as we strive toward the development of an optimal communication interface with neural tissue.

APPENDIX

Here the procedure used in the fabrication of our devices is described. Also given are the capacitance measurement and the noise measurement circuits. First we list four cleaning processes which recur often in integrated circuit processing so that in the procedure outline we may refer to them by name. We also list the etchants used for oxide and metal patterning.

I-clean - for initial wafer oxidation

10 min. - #3 Stripping Solution @ 90-100°C
1 min. - Deionized water (DIH_2O)
15 sec. - Concentrated HF
1 min. - DIH_2O
10 min. - Nitric Acid
3 min. - DIH_2O
Dry with nitrogen blower

G-clean - for Boron deposition

10 min. - #3 Stripping Solution @ 90-100°C
1 min. - DIH_2O
15 sec. - 10:1 H_2O:HF
1 min. - DIH_2O
10 min. - Nitric Acid
3 min. - DIH_2O
Dry with N_2 Blower

D-clean - for Boron drive

45 sec - 10:1 H_2O:HF - to remove excess borosilicate glass
1 min. - DIH_2O
Dry with N_2blower
5 min. - #3 Stripping Solution @ 90-100°C
1 min. - DIH_2O
10 min. - Nitric Acid
3 min. - DIH_2O
Dry with N_2 blower

L-clean - for metalization

10 min. - #3 Stripping Solution @ 90-100°C
1 min. - DIH_2O
10 sec. - 20:1 Ammonium Flouride
1 min. - DIH_2O
Dry with N_2 blower

Buffered etch - for silicon dixode removal

1800ml 40% Ammonium Flouride
280ml HF

PAN etch - for aluminum

400ml Phosphoric acid
25ml Acetic acid
25ml Nitric acid
50ml DIH_2O

Gold etch

1 liter Methanol
250gm Potassium Iodide - allow solution time to saturate
250gm Iodine

Chrome etch

165.4gm Ceric Ammonium Nitrate
4.3ml Perchloric acid
Add DIH_2O to make one liter

Device Process

Substrate should be N-type with resistivity greater than or equal to 10ohm-cm.

1) I-clean
2) Oxidize - 1100°C 10 min.dry
45 min.wet
15 min.dry

3) Spin coat - KTFR 1:1 (resist:thinner) 6000RPM for 15 sec.

4) Prebake - 20 min. @ 90°C

5) Align and expose with mask level A (fig.3-12a)

6) Spray develop - 1min.

7) Postbake - 30 min @ 180°C

8) Buffered etch - approximately 7 min.

9) Strip photoresist

10) G-clean

11) Boron deposition - 950°C 1 hr.

12) D-clean

13) Boron drive - 1200°C 15 min.

14) I-clean (use 10:1 HF in step 3)

15) Oxodize - 1100°C
10 min dry
1 hr. wet (could raise to 2 hrs. for 1um oxide)
15 min.dry

16) Repeat 3)-9) only use mask level B (fig 3-12b)

17) L-clean

18) E-beam evaporation - 200Å chromium
15000Å gold*

19) Spin coat - Shipley 1350B 3000RPM 15 sec.

20) Prebake - 2 1/2 min 90°C

21) Repeat 19)-20)

22) Align and expose with mask level C (fig.3-13)

23) Develop 30 sec. Shipley 1350B dev.

24) Postbake - 30 min. 180°C

---

*Due to uneveness of the polyimide coating some parts of the wafer get exposed before the whole wafer is fully etched. Gold is susceptible to the O_2 plasma etch and a thinner coat of gold will get etched away.

25) Gold etch - 2 1/2-3 min with agitation

26) Rinse - methanol

27) Chrome etch - 30 sec.

28) Rinse - DIH_2O

29) Strip photoresist

30) Spin coat - polyimide surface promoter 6000RPM 15 sec.

31) Drop coat - DuPont Ultrapure 2555 Polyimide approximately 18 drops/6in^2(2in wafer) for a 50um coat. Smear until even with an eye dropper.

32) Air dry - 10 min. on a flat surface

33) Cure - 1 hr. 90°C
overnight 180°C (be sure to use flat surface)

34) Evaporation - 4000Å aluminum*

35) Repeat 19)-21)

36) Align moat pattern to electrodes through window in Al

37) Develop - 30 sec Shipley 1350B dev.

38) Postbake - 30 min 180°C

39) PAN etch - approximately 10-15 min.

40) Rinse - DIH_2O

41) Reactive ion etch - 80 Watts (1Kv p-p)
10^{-5} torr O_2 atmosphere
This step takes approximately 8 hours. Inspect at the halfway point and proceed accordingly. Etching past completion should be avoided.

---

*Be sure to use a thin strip of material (glass or silicon) to cover some of the devices. The window thus created will permit alignment of the moat mask to the underlying electrodes in step 36).

42) PAN etch - until residual aluminum of moat mask is removed

43) E-beam evaporation of backside 200Å chromium
5000Å gold

44) Dice wafer, attach glass coverslip, cable and silastic cuff.

Capacitance Measurement

The circuit used to measure an unknown capacitance, C_e in series with a known resistance, R_L is shown in figure A-1a. A 50mV* sine wave at 1000Hz is applied through a large coupling capacitor, C_T. The voltage output is measured and the ratio $V_{out}/V_{in} = K$ is calculated. C_e is obtained

$$\text{A.1} \quad C_e = 1.59\times10^{-4}K\,(10^8 - K^2(10^4+R_L)^2)^{-\frac{1}{2}}$$

where R_L is the diffusion lead resistance. For measurements in air, C_T was replaced by a short circuit. For measurements of electrode-saline capacitance, C_T was produced by a large surface area gold electrode as shown in figure A-1b. C_T was on the order of .1uF.

Noise Measurement

Noise measurement was accomplished using the circuit in figure A-2. A noise source (resistor etc.) was input to a high gain high impedance amplifier. The output of the amplifier was filtered appropriately (200Hz-10KHz BPF). The amplifier and

---

*Gesteland et al (1959) state that much larger voltages across a metal-saline interface may cause harmonic distortion and possibly irreversible effects at the interface.

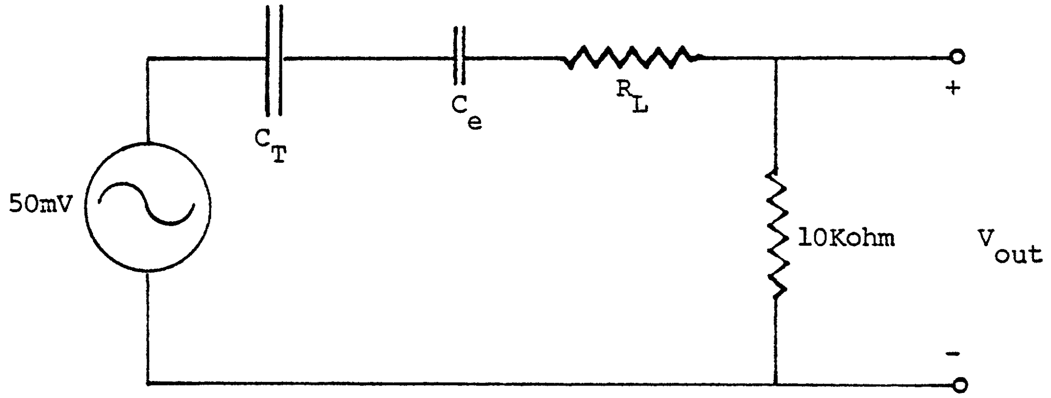

(a) circuit

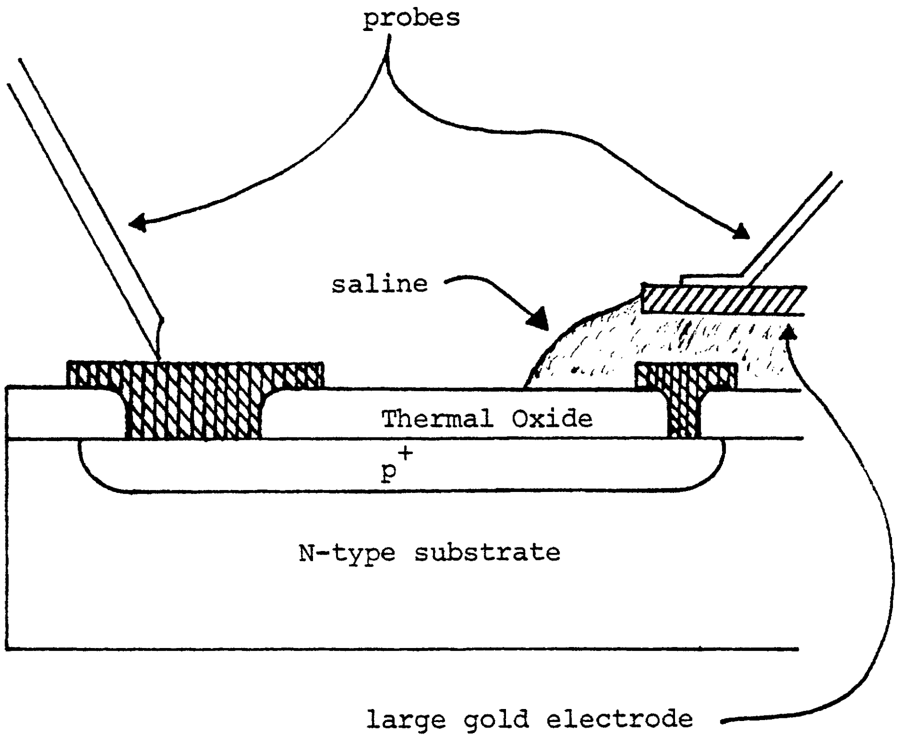

(b) electrode-saline capacitance measurement

Figure A-1: Capacitance measurement system.

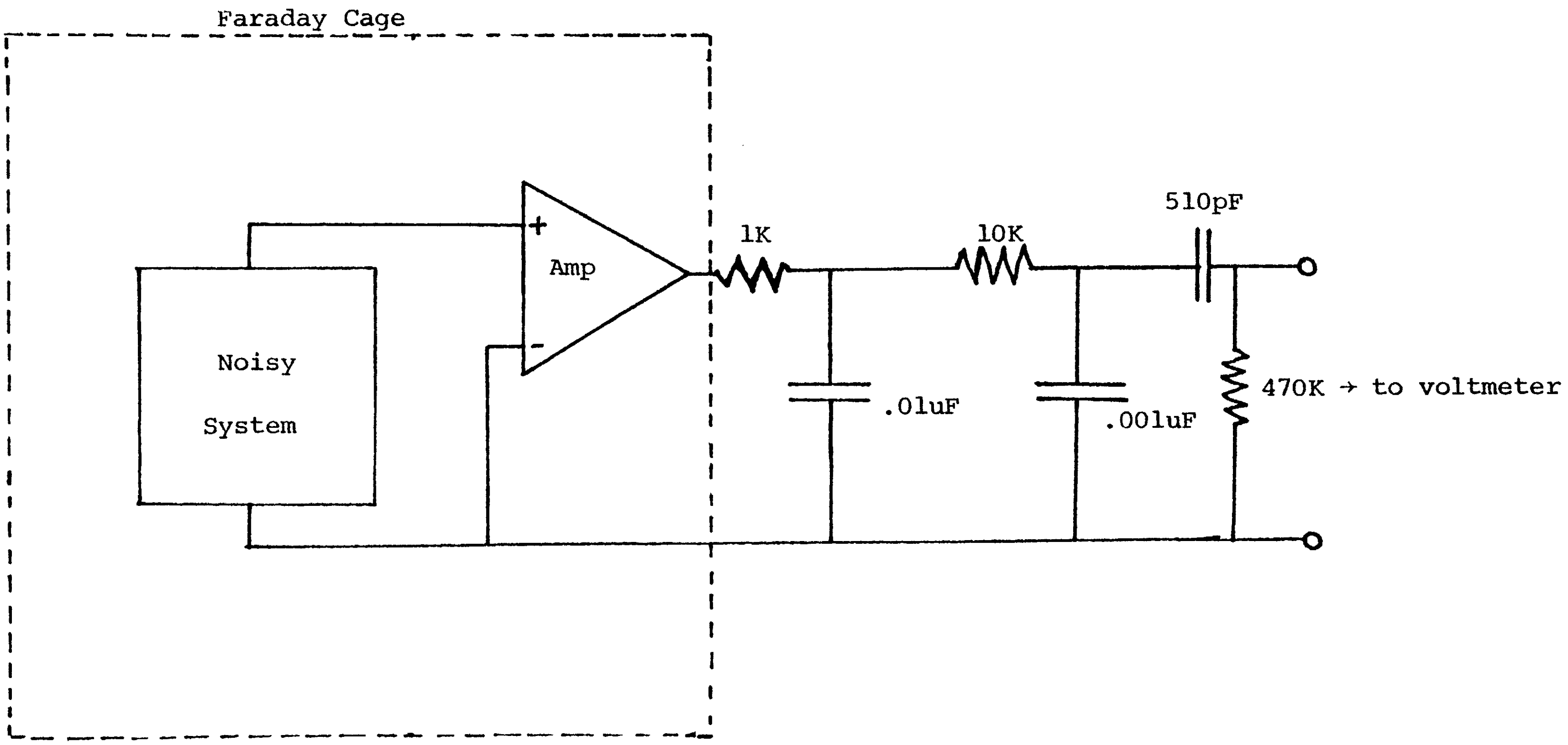

Figure A-2: Noise measurement system

noise source were shielded in a Faraday cage. The system was calibrated so that the gain from noise source to filter output in the pass band was 1000, thus 1uV at the noise source input produced 1mV at the filter output. The filter output was fed to a RMS voltmeter and the value read divided by 1000 to give the RMS value of the noise at the input to the amplifier.

The thermal RMS noise level generated by a resistor R is given by

A.2 $V_N = (4kTR\Delta F)^{\frac{1}{2}}$

k - Boltzman constant (1.38×10^{-23} joule/°K)

T - temperature in °K

ΔF - bandwidth in Hz

R - resistance in ohms

For a ΔF = 10KHz and T = 300°K, the expected values of V_N for 5Mohm, 500Kohm, 50Kohm and 0 ohm resistors is shown below. Also shown is the noise level measured by our system for precision resistors with these values.

R	V_N	Measured Noise
5Mohm	28.77uV	28.2uV
500Kohm	9.09uV	8.2uV
50Kohm	2.87uV	2.5uV
short	0uV	.13uV

Notice that the measured value for R=0 is non-zero. This noise generation occurred in the band-pass filter. If the input to the filter was open-circuited, the .13uV reading was still obtained. Mechanical considerations rendered the shileding of the filter in the Faraday cage difficult and since the accuracy of the system was not impaired for our purposes, no attempt was made to do so. Our expected signals from nerve fibers of 500uV should be clearly visible above the low noise level of less than .13uV of our electrodes.

REFERENCES

1 Andreassen, et al, Application of Optimal Multichannel Filtering to Simulated Nerve Signals, Biol.Cyber, 32(25) 1979.

2 Bassous, Fabrication of Novel Three-Dimensional Microstructures by the Anisotropic Etching of (100) and (110) silicon, IEEE Trans. on Electron Dev., vol.ED-25,#10, pp1178-1185, October, 1978.

3 Bean, Anisotropic Etching of Silicon, IEEE Trans. on Electron Dev., Vol. Ed-25,#10, pp1185-1193, October,1978.

4 Boretos, Concise Guide to Biomedical Polymers Their Design Fabrication and Molding, Charles C. Thomas, 1973.

5 Boyd & Davey, Composition of Peripheral Nerve, E & S Livingstone, 1968.

6 Bullock & Horridge, Structure & Function in the Nervous System of Invertebrates, W. H. Freeman, San Francisco,1965.

7 Calvin, W. H. Some Simple Spike Separation Techniques for Simultaneously Recorded Neurons, Electroencephalography & Clinical Neurophysiology, 1973, 34:94-96.

8 Campbell, et al, Regeneration of Adult Mammalian Spinal Cord, Science, 1957 (126) 929.

9 Colclaser, Microelectronics: Processing & Device Design, Wiley, 1980.

10 Cole, Membranes Ions and Impulse, Univ.of Cal. Press, 1968.

11 Davis, et al, Compound Action Potentials Recorded from Mammalian Peripheral Nerves Following Ligation or Resuturing., J. Physiol, 1978 (285) pp543-559

12 DeGraff & Flanders, Directional Oxygen Ion Beam Etching of Carbonaceous Materials, J. Vac. Sci. Technol., Nov/Dec 1979 16(6) p.1906.

13 DeLuca, C.J., Control of Upper Limb Prostheses: A Case for Neuroelectric Control, Journal of Med. Eng. & Tech. Vol.2. #2, 1978,pp57-61.

14 DeLuca & Gilmore, Voluntary Nerve Signals from Severed Mamallian Nerves: Long Term Recordings, Science,1978 (19) pp193-195.

15 DeLuca & Lichtenberg, Distinguishability of Functionally Distinct Evoked Neuroelectric Signals on the Surface of a Nerve, IEEE Trans.on BME, Vol.BME 26 #4, April 1979, pp228-237.

16 Dymond, Characteristics of the Metal Tissue Interface of Stimulation Electrodes, IEEE Trans. on BME, July 1976, pp274-280.

17 Edell, Development of a Chronic Neuroelectric Interface, Doctoral Dissertation, U.C. Davis, Winter 1980.

18 Ephrath & DiMaria, Review of RIE Induced Radiation Damage in Silicon Dioxide, Solid State Technology, Vol.24#1, April 1981, p182.

19 Florey, An Introduction to General & Comparative Animal Physiology, W.B. Saunders Co. 1966.

20 Gaal, Medgyesi & Vereczkey, Electrophoresis in the Separation of Biological Macromolecules, Wiley, 1980.

21 Gengerelli, et al, Magnetic Fields Accompanying Transmission of Nerve Impulses in the Frog's Sciatic, The Journal of Psychology, 1961 52 317-326.

22 Gesteland, Howland & Lettvin, Proceedings IRE, 1959 47 (1856).

23 Gordon, et al, Long Term Effects of Axotomy on Neural Activity During Cat Locomotion, J. Physiol, (303) Jun 243-263 (1980).

24 Gray & Searle, Electronic Principles; Physics, Models & Circuits, Wiley 1969.

25 Grove, Physics and Technology of Semiconductor Devices, Wiley, 1967.

26 Hamilton & Howard, Basic Integrated Circuit Engineering, McGraw-Hill 1975.

27 Harper, Handbook of Materials and Processes for Electronics, McGraw-Hill 1970.

28 Hawryluk, A., Personal Communication. Spring, 1981.

29 Jacobs & Cavanagh, Species Differences in Internode Formation Following Two Types of Peripheral Nerve Injury, Journal of Anatomy, 1969 Vol. 105(2) 295.

30 Langer, Controlled Release: A new Approach to Drug Delivery, Technology Review, Vol 83#5, 1981 pp26-34.

31 Levi-Montalcini & Angeletti, Nerve Growth Factor, Physiol. Rev. 1968 (48) pp534-569.

32 Lieberstein & Mahrous, A Source of Large Inductance and Concentrated Moving Magnetic Fields on Axons, Mathematical Biosciences, 7 (1970) pp41-60.

33 Leob, et al, Histological Reaction to Various Conductive and Dielectric Films Chronically Implanted in the Subdural Space, J. Biomed Mat. Res. Vol 11 1977 (195).

34 Mannard, Stein & Davis, Regeneration Electrode Units: Implants for Recording from Peripheral Nerve Fibers in Freely Moving Animals, Science, 1974 183 (547)

35 Marks & Loeb, Action Currents, Internodal Potentials and Extracellular Records of Myelinated Mammalian nerve Fibers Derived from Node Potentials, Biophysical J. 16 (655) 1976.

36 Maussel and Glang, Handbook of Thin Film Technology, McGraw-Hill 1970.

37 Nesmeianova, Experimental Studies in Regeneration of Spinal Neurons, Wiley-Halstead Press 1977.

38 Park & von Recum, Permanent Percutaneous Devices, CRC Critical Reviews in Bioeng. Vol. 5 #1 1981.

39 Peake, W.T., Verbal Communication, 4/24/81.

40 Prochazka,& Kornhuber, One Line Multiunit Sorting with Resolution of Superposition Potentials, Electroenceph.& Clin. Neurophys., 1973, 34:91-93.

41 Roberts & Hartline, Separation of Multiunit Nerve Impulse Trains by a Multichannel Linear Filter Algorithm, Brain Research, 94 (1975) 141-149.

42 Robinson, The Electrical Properties of Metal Microelectrodes, Proceedings of the IEEE, Vol. 56 #6 June, 1968, pp1065-1071.

43 Schanne & P.-Ceretti, Impedance Measurements in Biological Cells, Wiley 1978.

44 Schmidt, Unit Activity from Peripheral Nerve Bundles Utilizing Correlation Techniques. Medical & Biol. Eng. Vol.9 1971, pp665-674.

45 Scott & Clementi, Regeneration of Spinal Cord Fibers in the Cat, J. Compar. Neurol., 102,3, 1955, pp633-670.

46 Shapiro & Terry, Anodic Bonding Revisited, Stanford,E412, Dr. J.D. Meindl, Winter 1978.

47 Singer & Schade, Mechanisms of Neural Regeneration (Progress in Brain Research V.13), Elsevier 1964.

48 Stein, et al, Mathematical Analysis of Optimal Multichannel Filtering for Nerve Signals, Biol. Cyber, 32(19) 1979.

49 Stein, Charles, et al, Principles Underlying New Methods for Chronic Neural Recording, Le Journal Canadien de Sciences Neurologiques, August 1975 2 (235)

50 Stein & Pearson, Predicted Amplitude and Form of Action Potentials Recorded from Unmyelinated Nerve Fibers, J. Theor. Biol., 1971 32 (539-558).

51 Sunderland, Nerves and Nerve Injury, The Williams and Wilkins Co., Baltimore 1968.

52 30th ACEMB, Seven Briefs on CHEMFETs by various researchers, Los Angeles, Ca. November 1977, pp296-302.

53 Windle & Chambers, Regeneration in the Spinal Cord of the Cat and the Dog, J. Comp. Neurol., (1951) 93, 241-257.

54 Young, The Functional Repair of Nervous Tissue, Physiol. Rev. 22, 318-374 (1942).

BIOGRAPHY

Christopher Rose was born in New York City on January 9, 1957. He attended the Dalton School from 1968 to 1975.

He took his Bachelor of Science in Electrical Engineering at the Massachusetts Institute of Technology in June 1979.

In the Spring of 1979, he was awarded a Bell Laboratories Cooperative Research Fellowship and is currently engaged in doctoral studies at the Massachusetts Institute of Technology in the Department of Electrical Engineering and Computer Science.